Atmos. Chem. Phys. Discuss., 10, 30205–30277, 2010
www.atmos-chem-phys-discuss.net/10/30205/2010/
doi:10.5194/acpd-10-30205-2010

Atmospheric Chemistry and Physics Discussions

Modeling organic aerosols in a megacity: comparison of simple and complex representations of the volatility basis set approach

M. Shrivastava[1], J. Fast[1], R. Easter[1], W. I. Gustafson Jr.[1], R. A. Zaveri[1], J. L. Jimenez[2], P. Saide[3], and A. Hodzic[4]

[1]Atmospheric Sciences & Global Change Division, Pacific Northwest National Laboratory, Richland, WA 99352, USA
[2]University of Colorado, Boulder, CO, USA
[3]Center for Global and Regional Environmental Research, University of Iowa, Iowa City, IA, USA
[4]National Center for Atmospheric Research, Boulder, CO, USA

Received: 20 October 2010 – Accepted: 27 November 2010 – Published: 10 December 2010

Correspondence to: M. Shrivastava (manishkumar.shrivastava@pnl.gov)

Published by Copernicus Publications on behalf of the European Geosciences Union.

Abstract

The Weather Research and Forecasting model coupled with chemistry (WRF-Chem) is modified to include a volatility basis set (VBS) treatment of secondary organic aerosol formation. The VBS approach, coupled with SAPRC-99 gas-phase chemistry mechanism, is used to model gas-particle partitioning and multiple generations of gas-phase oxidation of organic vapors. In addition to the detailed 9-species VBS, a simplified mechanism using 2 volatility species (2-species VBS) is developed and tested for similarity to the 9-species VBS in terms of both mass and oxygen-to-carbon ratios of organic aerosols in the atmosphere. WRF-Chem results are evaluated against field measurements of organic aerosols collected during the MILAGRO 2006 campaign in the vicinity of Mexico City. The simplified 2-species mechanism reduces the computational cost by a factor of 2 as compared to 9-species VBS. Both ground site and aircraft measurements suggest that the 9-species and 2-species VBS predictions of total organic aerosol mass as well as individual organic aerosol components including primary, secondary, and biomass burning are comparable in magnitude. In addition, oxygen-to-carbon ratio predictions from both approaches agree within 25%, providing evidence that the 2-species VBS is well suited to represent the complex evolution of organic aerosols. Model sensitivity to amount of anthropogenic semi-volatile and intermediate volatility (S/IVOC) precursor emissions is also examined by doubling the default emissions. Both the emission cases significantly under-predict primary organic aerosols in the city center and along aircraft flight transects. Secondary organic aerosols are predicted reasonably well along flight tracks surrounding the city, but are consistently over-predicted downwind of the city. Also, oxygen-to-carbon ratio predictions are significantly improved compared to prior studies by adding 15% oxygen mass per generation of oxidation; however, all modeling cases still under-predict these ratios downwind as compared to measurements, suggesting a need to further improve chemistry parameterizations of secondary organic aerosol formation.

ACPD

10, 30205–30277, 2010

1 Introduction

Organic aerosol (OA) comprises a large fraction (20 to 90%) of submicron particulate matter in the atmosphere affecting radiative climate forcing and human health (Murphy et al., 2006; Zhang et al., 2007). Accurate representation of OA in models requires a good understanding of processes leading to formation and removal of OA in the atmosphere. OA is composed of directly emitted primary organic aerosols (POA) and photochemically produced secondary organic aerosols (SOA). POA is emitted from a variety of sources such as fossil fuel and biomass burning.

POA has traditionally been considered as non-volatile and non-reactive in air quality models. However, recently Robinson et al. (2007) showed that instead of a static fixed non-volatile mass, POA is a dynamic system formed due to gas-particle mass transfer of a multi-component mixture of semi-volatile organic species evolving as a function of atmospheric variables such as dilution, temperature, and pre-existing OA as predicted by absorptive partitioning theory (Shrivastava et al., 2006). Thus, the conceptual model of Robinson et al. (2007) emits organic precursors which are lumped into nine surrogate volatility species separated by factor of 10 at 298 K (volatility basis set or VBS) classified as: (1) semi-volatile organic compounds (SVOC) with effective saturation concentrations (C^*) ranging 10^{-2} to 10^3 $\mu g\,m^{-3}$ and (2) intermediate volatility organic compounds (IVOC) with C^* ranging 10^4 to 10^6 $\mu g\,m^{-3}$. A substantial portion of SVOC mass will partition to POA in the atmosphere, while in the absence of photochemistry, the IVOC species remain as organic vapors under most atmospheric conditions. This multi-component mixture of SVOC and IVOC (S/IVOC) species is assumed to undergo gas-phase photochemical oxidation by OH radicals resulting in formation of successively lower volatility species, which may condense to form SOA (Robinson et al., 2007; Shrivastava et al., 2006).

SOA formation also occurs through gas-phase oxidation of volatile organic compounds (VOCs with C^* greater than 10^7 $\mu g\,m^{-3}$) such as biogenic VOCs (e.g., terpenes and isoprene) and traditional anthropogenic VOCs (e.g., aromatics and higher

ACPD
10, 30205–30277, 2010

MW alkanes and olefins) (Tsimpidi et al., 2010). However, SOA formation through oxidation of S/IVOC precursors is thought to be more efficient as compared to VOC precursors, as S/IVOC species have lower volatility favoring partitioning to the particle phase after oxidation (Donahue et al., 2006). In light of this scientific understanding, POA is more completely defined as particulate matter either directly emitted, or formed in the atmosphere from freshly emitted relatively reduced organic vapors due to gas-particle partitioning, before photochemical oxidation. SOA is defined as particulate matter formed after single to multi-generational photo-chemical oxidation of S/IVOC precursors ("SI-SOA") or biogenic/traditional anthropogenic VOCs ("V-SOA") in the atmosphere following the terminology of Tsimpidi et al. (2010).

Aerosol Mass Spectrometer (AMS) measurements and subsequent analysis with Positive Matrix Factorization (PMF) classify total OA as hydrocarbon-like OA (HOA representing fresh OA), and oxygenated OA (OOA representing OA formed after chemical oxidation in the atmosphere) (Ulbrich et al., 2009). HOA and OOA have been shown to be good surrogates of urban POA and total SOA, respectively, in the atmosphere (Zhang et al., 2007). Recent results show that SOA accounts for a large fraction of OA burden throughout the atmosphere with its fraction of total OA increasing from urban to remote continental locations (Zhang et al., 2007). Previous "bottom up" chemical transport models based on parameterizations derived from laboratory experiments severely under-predicted the magnitude and evolution of SOA in polluted regions (de Gouw et al., 2005; Goldstein and Galbally, 2007; Hallquist et al., 2009; Heald et al., 2005; Volkamer et al., 2006), while predictions in unpolluted biogenically-dominated regions do not show a similar under-prediction (Slowik et al., 2010; Tunved et al., 2006). Recent modeling efforts have significantly increased the amount of SOA modeled in polluted regions, bringing model predictions closer to measurements (Dzepina et al., 2009; Hodzic et al., 2010a). Using a box model and data from the MCMA-2003 campaign, Dzepina et al. (2009) combined different modeling approaches to close the gap between model and measurements for SOA. Dzepina et al. (2009) found that SOA resulting from photochemical oxidation of S/IVOC precursors accounted for about half

ACPD
10, 30205–30277, 2010

of the observed SOA mass. However, large uncertainties remain in terms of various model parameters and other SOA formation pathways and yields. Recently some models have been proposed which "age" semivolatiles formed in V-SOA mechanisms by gas-phase reaction, as in e.g. Tsimpidi et al. (2010). However, Dzepina et al. (2010) recently reported that the Tsimpidi et al. (2010) mechanism produces enough SOA to match the regional observations, and that a large SOA overprediction is observed when SI-SOA is also implemented.

In addition to mass, aerosol hygroscopicity is an important parameter affecting direct and indirect radiative forcing of climate. The hygroscopicity parameter κ was recently shown to be directly related to elemental oxygen to carbon molar ratios of OA (O:C ratio) for ambient aerosols in urban, remote and forest locations (Jimenez et al., 2009). Most of the large-scale chemical transport models are not designed to represent the O:C ratio of OA due to complexity of processes involved. Measurements of O:C ratio with the High-Resolution Time-of-flight Aerosol Mass Spectrometer (HR-ToF-AMS) have recently become available as an indicator of oxidation state of OA in the atmosphere. Only recently, attempts have been made to predict the O:C ratio of OA (Dzepina et al., 2009; Hodzic et al., 2010a). Both studies found that the ROB (Robinson et al., 2007) approach under-predicted the ambient O:C, while the GRI (Grieshop et al., 2009) approach was a better fit to the observations. However the very rapid addition of oxygen postulated in the GRI mechanism is inconsistent with known gas-phase chemistry. SOA from glyoxal can also increase O:C (Dzepina et al., 2009). These knowledge gaps suggest that even though models are getting closer to representing the mass of SOA, they may be getting the right answers for the wrong reasons or as a result of compensating errors from various SOA mechanisms. This calls for a continuing need for measurements designed to constrain model representations of SOA.

Prediction of O:C ratios also requires separate tracers for carbon and oxygen species for both freshly emitted and oxidized organic species in the atmosphere, with each class of organics (such as fresh, oxidized) being represented by a separate VBS of 8 or 9 volatility intervals (Hodzic et al., 2010a; Shrivastava et al., 2008). In chemical

ACPD
10, 30205–30277, 2010

transport models, advection of this large set of organic species requires more computational time than chemistry and gas-particle partitioning combined. Models running online meteorology, such as the Weather Research and Forecasting Model coupled to chemistry (WRF-Chem) (Grell et al., 2005), are especially susceptible to this large computational burden as compared to offline representations of meteorology in chemical-transport models, such as CHIMERE (Hodzic et al., 2009) and CMAQ (Carlton, 2010), because the advection time step is similar for meteorology and chemistry. An important advantage of online models is that they permit aerosol-radiation-cloud-chemistry interaction processes and the associated feedback effects on meteorology to be simulated, whereas offline models cannot study these processes.

The objectives of this work are to: (1) implement a detailed OA mechanism in WRF-Chem based on a 9-species VBS that includes SOA formation from S/IVOC precursors (Robinson et al., 2007) and traditional anthropogenic/biogenic VOCs; (2) modify the ROB mechanism in terms of oxygen added per generation of oxidation and test predictions of O:C ratios; (3) develop a highly condensed 2-species SOA mechanism and evaluate it in terms of performance and computational speed compared to the more detailed VBS mechanism; and (4) evaluate the OA mechanisms using field measurements of organic aerosols collected during the 2006 MILAGRO field campaign in the vicinity of Mexico City.

We will show that it is possible to successfully develop highly condensed OA mechanisms that give very similar results to the detailed VBS mechanisms and are more suitable for real-time forecasting and climate model applications. It is also extremely important to test simplified organic aerosol mechanisms using a model configuration that can resolve much of the temporal and spatial variations of observed organic aerosols, before these mechanisms are routinely used in global models with coarse spatial resolution that are difficult to evaluate using point measurements. The terminology used for various classes of organic species used in this study is described in Table 1 for reference.

ACPD
10, 30205–30277, 2010

2 Model description

Version 3.1.1 of the WRF-Chem community model is used to simulate the atmospheric conditions between 6 and 30 March 2006 over Mexico. Trace gases and aerosols are simulated simultaneously with meteorology (Grell et al., 2005). WRF-Chem includes several options for gas-phase chemistry and aerosols. In this study, gas-phase chemistry is represented by the SAPRC-99 mechanism (Carter, 2010) and the aerosol lifecycle processes are represented by the MOSAIC aerosol module (Zaveri et al., 2008). Aerosol species in MOSAIC includes sulfate, nitrate, ammonium, sodium, chloride, calcium, carbonate, other inorganics (i.e. dust), methanesulfonate, elemental carbon, organic matter, and aerosol water; however, until now organic matter has been treated as non-volatile POA. Additional details of the WRF-Chem model have been described previously (Fast et al., 2009). Here, only processes and modifications to WRF-Chem relevant to simulating organic aerosol components are described in detail. The 9-species VBS mechanism for organic aerosols implemented in WRF-Chem is described first, followed by a discussion of the assumptions needed to develop a condensed 2-species mechanism.

2.1 Detailed 9-species VBS mechanism for OA

The 9-species VBS mechanism for POA and non-traditional SOA implemented in WRF-Chem is similar to that described by Robinson et al. (2007) and Shrivastava et al. (2008), with modifications for global non-volatile fraction and amount of oxygen added per generation of oxidation as described later. Previous studies have already implemented versions of this mechanism using offline meteorological models (Hodzic et al., 2010a; Tsimpidi et al., 2010).

The mechanism treats POA species as 9 surrogate species with C^* values (at 298 K and 1 atm) of 10^{-2}, 10^{-1}, 10^{0}, 10^{1}, 10^{2}, 10^{3}, 10^{4}, 10^{5}, 10^{6} μg m^{-3}. For each surrogate species, we treat both the aerosol phase species (in 4 size bins for this study) and the gas phase species. The bin boundaries for the size bins are 0.0391, 0.156,

ACPD
10, 30205–30277, 2010

0.625, 2.50, and 10.0 µm (dry diameter). Aerosol phase species for higher volatility ($>10^4$ µg m^{-3}) could be neglected with little effect on OA predictions, but were included for completeness. In future applications, aerosol species of higher volatility would be excluded from WRF-Chem to save computational time. The POA species are segregated by two emissions sectors: biomass burning and anthropogenic (predominately fossil fuel). To allow calculating O:C ratios for the modeled OA, separate model species are used for the oxygen and non-oxygen (C, H, N) components of each species. This gives the following POA species:

- POA(a)$_{i,e,x,n}$ = aerosol-phase POA, where i is the volatility species (1–9), e is either the biomass or anthropogenic emission sector, x is either the oxygen or non-oxygen component, and n is the size bin (1–4).
- POA(g)$_{i,e,x}$ = corresponding gas-phase POA species.

Partitioning between the gas and aerosol phase species is calculated using absorptive partitioning theory assuming thermodynamic equilibrium approach as described by Donahue et al. (2006).

The O:C ratio of bulk particulate OA evolves as a function of emissions of fresh primary organic material, oxidation of organic vapors with addition of oxygen mass after each generation of oxidation (Robinson et al., 2007), gas-particle partitioning varying with ambient factors such as temperature, dilution and OA concentrations, and removal rates of OA and gas-phase semi-volatiles due to dry and wet deposition. An OM/OC (organic mass to organic carbon ratio) of 1.57 and 1.25 for biomass burning and anthropogenic emissions respectively is assumed, converting OM emission rates to OC. Elemental O:C ratios of 0.3 and 0.06 are assumed for fresh biomass burning and anthropogenic emissions for calculating the oxygen fraction of each species. In addition, non-oxygen (carbon, hydrogen and nitrogen) to carbon ratio of 1.17 was assumed for all species. These assumptions are consistent with PMF analysis of ambient AMS data by Aiken et al. (2008) in Mexico City. The sum of oxygen and non-oxygen parts for each species equals total OM input to WRF-Chem, thus all OM mass is accounted

ACPD
10, 30205–30277, 2010

for in the gas-particle partitioning calculations. The gas-phase POA species react with OH to produce more-oxygenated and lower-volatility SI-SOA species, as described in Sect. 2.1.2.2. These SI-SOA species are represented in the mechanism by SI-SOA(a)$_{i,e,x,n}$ and SI-SOA(g)$_{i,e,x}$, for $i = 1,8$ representing 8 oxidized volatility species as described by Shrivastava et al. (2008).

In addition to the 9-species VBS mechanism for POA and non-traditional SOA, we include a 4-species VBS treatment of traditional SOA (referred to as V-SOA) produced by oxidation of biogenic and traditional anthropogenic VOCs. V-SOA C^* ranges from 1 to 10^4 μg m^{-3}. We segregate the V-SOA species by the parent-VOC emissions sector (biogenic and traditional anthropogenic). This gives the following V-SOA species:

V-SOA(a)$_{i,e,n}$ = aerosol-phase V-SOA, where i is the volatility species (1–4), e is either the biogenic or traditional anthropogenic emission sector, and n is the size bin (1–4).

– V-SOA(g)$_{i,e}$ = corresponding gas-phase V-SOA species.

The mechanism does not treat further oxidation of the V-SOA gas-phase species, so separate model species for oxygen and non-oxygen component are not required for calculating O:C ratios. Instead, we assume a fixed OM:OC (mass) ratio of 1.90 and O:C (elemental) ratio of 0.4 for V-SOA (Aiken et al., 2008).

Overall, there are 180 POA species (36 gas, 144 aerosol), 160 SI-SOA species (32 gas, 128 aerosol), and 40 V-SOA species (8 gas, 32 aerosol) in the mechanism. The total SOA formed at any time within the modeling domain is the sum of SI-SOA and V-SOA after gas-particle partitioning calculations.

2.1.1 Emissions

An updated anthropogenic emissions inventory is used for MILAGRO 2006 from the work of Song et al. (2010). The anthropogenic emissions inventory includes traffic emissions and municipal trash burning. Municipal trash burning emissions are estimated to be comparable in magnitude to traffic emissions, but most of the trash burning

ACPD
10, 30205–30277, 2010

sources are located outside the city. Also, municipal trash burning is expected to have similar OA spectra as fresh vehicular emissions dominated by hydrocarbon-like OA (HOA) with also some similarities with BBOA (Mohr et al., 2009); hence organic OA emissions from these sources are lumped together. BBOA represents primary biomass burning OA emissions.

Biomass burning estimates are derived from satellite remote sensing data. Emissions of gases and particles from open burning were calculated using the Fire inventory from NCAR version 1. This method is based on the estimation framework described by Wiedinmyer et al. (2006). Fire counts (MODIS Data Processing System, MODAPS) were provided by the University of Maryland (Giglio et al., 2003; MODIS Rapid Response Project). Land cover was determined with the MODIS Land Cover Type product (Friedl et al., 2010) and fuel loadings from Hoezelman et al. (2004). Emission factors were taken from multiple sources (Andreae and Merlet , 2001; M. O. Andreae, personal communications, 2008). The non-methane organic compounds were speciated to the SAPRC-99 mechanism based on species-specific emission factors and the ecosystem type in which the fire burned.

Representation of biomass burning within models is uncertain due to errors arising from calculations of plume rise, horizontal mixing of point sources and also due to the fact that several small fires may not be captured by remote sensing data (Fast et al., 2009). SVOC and IVOC emissions corresponding to both anthropogenic and biomass burning emissions are derived as follows:

Total SVOC emissions (organic vapors with C^* of 0.01–10^4 $\mu g\,m^{-3}$) are estimated as 3 times POA emissions for both anthropogenic and biomass burning emissions in Mexico City following Hodzic et al. (2010a) and Tsimpidi et al. (2010). This estimate is uncertain due to the fact that it is unclear what portion of SVOCs is represented by traditional POA emission inventory, and also that POA emission inventory itself is uncertain. The total SVOC emissions are then distributed among different volatility species with C^* ranging 0.01–10^4 $\mu g\,m^{-3}$ using the mass fractions suggested by Robinson et al. (2007) with one modification. Recently, Cappa and Jimenez (2010) found that a

ACPD
10, 30205–30277, 2010

significant fraction of OA emissions in Mexico City was globally non-volatile i.e. it would remain in particle phase under all ambient conditions. Using the default volatility distribution from Robinson et al. (2007) in the CHIMERE model, Hodzic et al. (2010a) found that POA was too volatile downwind of Mexico City. In this work, using the globally non-volatile fraction suggested by Cappa and Jimenez (2010), 9% of SVOC emissions from biomass burning and 22% of SVOC emissions from anthropogenic sources are represented by the lowest volatility species with C^* of 0.01 $\mu g\,m^{-3}$ thus rendering this fraction to be non-volatile under all relevant ambient conditions in and around Mexico City. It should be noted that this assumption did not change the volatility distribution for biomass burning emissions used by Hodzic et al. (2010a). Hodzic et al. (2010a) applied 3% fraction to 3 times POA emissions, which is equal to 9% fraction used for biomass carbon as shown in Table 2 in this work. Also, the volatility distribution for anthropogenic carbon used in this work is similar to biomass carbon, except the use of 23% emissions for the species with the C^* of 0.01 $\mu g\,m^{-3}$. The IVOC emissions (organic vapors with C^* of 10^4–10^6 $\mu g\,m^{-3}$ as shown in Table 1) are estimated as 1.5 times SVOC emissions (4.5 times traditional POA emissions) for both biomass burning and anthropogenic emission sources consistent with Robinson et al. (2007). Thus, the sum of all SVOC and IVOC precursors in the inventory is 7.5 times the mass of traditional POA emissions inventory. Addition of this large pool of S/IVOC precursors to the inventory is supported by an observed gap between measured OH reactivity and calculated OH reactivity based on known VOC precursors in Mexico City (Dzepina et al., 2009). Table 2 shows the mass factors (f_i) used to calculate S/IVOC emissions from POA emissions (converted to OC) in each category. The distributions for biomass and anthropogenic emissions differ due to assumption of global non-volatile fraction. These are further classified as oxygen and non-oxygen parts using respective factors as described in Sect. 2.1.

The MEGAN (Model of Emissions of Gases and Aerosols from Nature, http://bai.acd.ucar.edu) model (Guenther et al., 2006) is used to generate biogenic emissions in the modeling domain within and around Mexico City. The 138 biogenic species

ACPD
10, 30205–30277, 2010

from MEGAN are lumped into 3 biogenic VOC classes: isoprene (ISOP), terpenes (TERP) and sesquiterpenes (SESQ). In addition, anthropogenic VOC emissions including lumped classes corresponding to alkanes (ALK4 and ALK5), olefins (OLE1 and OLE2), and aromatics (ARO1 and ARO2) are included in the inventory corresponding to the SAPRC-99 mechanism, as described by Tsimpidi et al. (2010). Isoprene and terpene emissions calculated by the NEI emissions inventory for Mexico domain are removed to avoid double counting of biogenic emissions (already calculated by MEGAN model within the domain). This also removes the anthropogenic isoprene emissions within the modeling domain. Hodzic et al. (2009) showed that anthropogenic isoprene emissions were much larger (up to a factor of 5 higher) than biogenic isoprene emissions at the T0 site within Mexico City. But Hodzic et al. (2009) also pointed out that largest contribution to biogenic SOA within Mexico City basin was due to regional isoprene (>60%) produced upwind on the coastal areas and advected into the city.

2.1.2 Gas phase chemistry

All gas-phase chemistry equations leading to ozone and SOA formation are included within the Kinetic Pre-Processor (KPP) in WRF-Chem (Damian et al., 2002). The SAPRC-99 mechanism includes 211 reactions of 56 gases and 18 free radicals. This mechanism is updated to include gas-phase oxidation of various S/IVOC precursors forming SOA (A-SI-SOA and BB-SI-SOA for anthropogenic and biomass burning SI-SOA, respectively), and SOA formed due to oxidation of VOC precursors from traditional anthropogenic and biogenic emissions (A-V-SOA and B-V-SOA, respectively). The detailed treatment of OA has been fully integrated with the inorganic MOSAIC aerosol module in WRF-Chem, thus constituting a state-of-the-art representation of processes leading to organic and inorganic aerosol formation in the atmosphere. This detailed modeling approach in WRF-Chem is necessary to understand the suite of complex physical and chemical interactions between biogenic SOA formation, anthropogenic OA and inorganic species.

ACPD
10, 30205–30277, 2010

2.1.2.1 SI-SOA formation

Observations suggest continued SOA production as pollutants leave the Mexico City basin during low biomass burning periods (DeCarlo et al., 2008; Kleinman et al., 2008). Thus, multi-generational SOA chemistry is supported by ambient observations. SI-SOA formation from multi-generational gas-phase oxidation of S/IVOC precursors are calculated using oxidation parameters proposed by Robinson et al. (2007) with one modification. The mass of parent SVOC or IVOC species is assumed to increase by 15% for each generation of oxidation to account for added oxygen mass or functionalization. This is equivalent to assuming that 2 atoms of oxygen are added to an equivalent C_{15} H_{32} precursor per generation of oxidation. In comparison, Robinson et al. (2007) assumed an addition of 7.5% mass due to added oxygen. The oxidation mechanism proposed by Robinson et al. (2007) was not designed to predict the oxidation state of OA in the atmosphere. Use of 7.5% added oxygen mass has been shown to severely under-predict the O:C ratios in the atmosphere (Hodzic et al., 2010a). Jimenez et al. (2009) suggested that 1 to 3 oxygen atoms could be added per generation of oxidation. Grieshop et al. (2009) used 40% increase in mass due to addition of oxygen per generation of oxidation for wood smoke. Thus, the addition of 2 oxygen atoms is a fairly conservative assumption improving O:C ratio predictions as compared to 1 oxygen atom added by Robinson et al. (2007). An OH reaction rate constant of 4×10^{-11} cm^3 $molecule^{-1}$ s^{-1} is assumed for all SVOC and IVOC species.

The equations governing oxidation of S/IVOC precursors are written within the KPP module of WRF-Chem as follows:

$$POA(g)_{i,e,c} + OH \rightarrow SI-SOA(g)_{i-1,e,c} + 0.15SI-SOA(g)_{i-1,e,o} \quad (1)$$

$$POA(g)_{i,e,o} + OH \rightarrow SI-SOA(g)_{i-1,e,o} + OH \quad (2)$$

$$SI-SOA(g)_{i,e,c} + OH \rightarrow SI-SOA(g)_{i-1,e,c} + 0.15SI-SOA(g)_{i-1,e,o} \quad (3)$$

$$SI-SOA(g)_{i,e,o} + OH \rightarrow SI-SOA(g)_{i-1,e,o} + OH \quad (4)$$

ACPD
10, 30205–30277, 2010

where i denotes any given volatility species except the lowest volatility, $i-1$ denotes the species with C^* equal to $i/10$, e denotes the source type, and subscripts c and o represent the non-oxygen and oxygen parts respectively of given species. As shown by Eqs. (1) and (3), oxidation of non-oxygen part of SI-SOA precursor i results in formation of non-oxygen and oxygen parts (15% by mass for 2 oxygen atoms added) of SI-SOA with successive lower volatility $i-1$. Since molecular weights of all VBS species are assumed as 250 g mole^{-1} mass yields are same as molar yields, so 0.15 is used as oxygen yield per oxidation step within KPP. Equations (2) and (4) depict movement of oxygen part of each precursor to lower volatility. Thus at any time, both non-oxygen and oxygen parts of any given species move to successively lower volatility species due to oxidation, satisfying mass conservation. The lowest volatility species (C^* equal to 0.01 µg m^{-3}), was assumed to be non-reactive, neglecting fragmentation reactions, following Robinson et al. (2007). In Eqs. (2) and (4), OH was added to both sides of the equations to make sure that OH loss is not double counted by oxidation of non-oxygen and oxygen parts of the same species.

2.1.2.2 V-SOA formation

SOA formation from biogenic and traditional anthropogenic VOCs (V-SOA) is represented using fixed yields of these species using a 4-product VBS following Tsimpidi et al. (2010). For alkane and olefin species mass yields are similar to Tsimpidi et al. (2010). For aromatic species yields from Hildebrandt et al. (2009) are implemented. Aging of VOCs in the gas-phase could be represented by the following equation:

$$\mathrm{VOC(g)}_i + \mathrm{OH} \rightarrow \sum_{i=1}^{n} a_i \mathrm{V-SOA(g)}_{i-1} \quad (5)$$

$$a_i = a_{i,\mathrm{high}} B + a_{i,\mathrm{low}} (1-B) \quad (6)$$

where i is the volatility species, a_i is the overall NO_x dependent molar yield calculated from Eq. (6), $a_{i,\mathrm{high}}$ and $a_{i,\mathrm{low}}$ are the molar yields under high and low NO_x conditions

ACPD
10, 30205–30277, 2010

respectively, B is the NO_x branching ratio as defined by Lane et al. (2008), and V-SOA(g)$_i$ is the gas phase V-SOA precursor concentration. The reaction rates of various VOC species with the OH radicals in Eq. (5) are already present within the SAPRC-99 mechanism, as a part of gas-phase chemistry.

Formation of V-SOA(a)$_i$ is represented by gas-particle partitioning of V-SOA(g)$_i$ defined by absorptive partitioning theory as discussed by Donahue et al. (2006). However, in contrast to Tsimpidi et al. (2010) "no further aging" of the V-SOA(g)$_i$ species is implemented in WRF-Chem as including it leads to larger regional over-prediction of SOA (Dzepina et al., 2010). Aging parameterizations based on smog chamber measurements are very uncertain as they try to predict SOA formation over longer time-scales (photochemical ages) than so far have been accessible in chambers (Ng et al., 2010). Smog chamber measurements need to be carried out to much longer time-scales (over several days) and OH exposures to quantify and parameterize multi-generational V-SOA formation from both biogenic and traditional anthropogenic precursors.

In this work, V-SOA yields are NO_x dependent as described by Tsimpidi et al. (2010). Table 3 lists mass yields of various V-SOA precursors represented by the 4-product VBS species V-SOA(g)$_i$. Molar yields are required as the SAPRC-99 mechanism lists equations and reaction rates in molecular units within the Kinetic Pre-Processor (KPP) in WRF-Chem. Mass yields listed in Table 2 are converted to molar yields by multiplying them with the ratio of molecular weights of V-SOA(g)$_i$ species (assumed to be 250 g mole^{-1}) and the corresponding VOC(g) precursors taken from the CAMx User's guide for SAPRC 1999 mechanism (CAMx vs. 5.10 User's guide, 2009). The assumed enthalpy of vaporization ΔH_{vap} for the V-SOA(g)$_i$ species are equal to respective volatility in Table 1.

2.2 Condensed 2-species OA mechanism

As discussed earlier, the addition of a large number of species represents a huge computational burden in terms of advection alone. Development of a condensed 2-species

ACPD
10, 30205–30277, 2010

mechanism is attractive for computational efficiency in large-scale global simulations. In this section, assumptions and parameterizations for development of the condensed 2-species mechanism within WRF-Chem are discussed.

The condensed mechanism represents POA by two volatility species with C^* values (at 298 K and 1 atm) of 10^{-2} and 10^5 μg m^{-3}, respectively. Separate POA species are used to represent the two emissions sectors and the oxygen and non-oxygen (C, H, N) components of each species as described in Sect. 2.1 above. This gives the following:

- POA(a)$_{i,e,x,n}$ = aerosol-phase POA, where i is the volatility species, e is either the biomass or anthropogenic emission sector, x is either the oxygen or non-oxygen component, and n is the size bin (1–4) as described in Sect. 2.1.
- POA(g)$_{i,e,x}$ = corresponding gas-phase POA species.

The gas-phase POA(g)$_{i=2,e,x}$ species (C^* of 10^5 μg m^{-3}) reacts with OH to produce SI-SOA(a)$_{i=1,e,x,n}$ and SI-SOA(g)$_{i=1,e,x}$(C^* of 10^{-2} μg m^{-3}). Note that both POA(a) and SI-SOA(a) in the condensed mechanism would remain in the aerosol phase under most atmospheric conditions due to low volatility.

In addition to the 2-species VBS mechanism for POA and non-traditional SI-SOA, we include a 1-species treatment of traditional SOA (referred to as V-SOA) produced by oxidation of biogenic and traditional anthropogenic VOCs. V-SOA C^* is assumed to be equal to 1 μg m^{-3} corresponding to the lowest volatility species in Sect. 2.1.2.2. We segregate the V-SOA species by the parent-VOC emissions sector (biogenic and traditional anthropogenic) giving V-SOA(a)$_{i=1,e,n}$ and V-SOA(g)$_{i=1,e}$ as described in Sect. 2.1.2.2.

In the condensed mechanism, there are 40 POA species (8 gas, 32 aerosol), 20 SI-SOA species (4 gas, 16 aerosol), and 10 V-SOA species (2 gas, 8 aerosol) in the mechanism.

ACPD
10, 30205–30277, 2010

2.2.1 S/IVOC emissions

The condensed 2-species approach represents POA and SOA as the first volatility species with C^* of 10^{-2} µg m^{-3}. This approach assumes that both POA and SOA in the model are non-volatile under most atmospherically relevant conditions. POA emissions are assumed to be 1/3rd of SVOC emissions in the 9-species VBS approach discussed in Sect. 2.1.1, allowing 2/3rd of SVOC emissions to have already evaporated relative to 9-species VBS approach, thus implicitly accounting for gas-particle partitioning. IVOC emissions (equal to 6.5 times POA) and 2/3rd of SVOC emissions are represented as the 2nd IVOC species with of C^* of 10^5 µg m^{-3}. The 2nd species represents all gas phase S/IVOC emissions within the modeling domain. Hence C^* for this species is chosen to be in the IVOC range to ensure all material remains in the gas phase under most atmospheric conditions. The total SVOC and IVOC emissions in the 2-species VBS approach are equal to the 9-species VBS. Table 4 shows the factors (f_i) used to calculate S/IVOC emissions from POA. As discussed earlier POA emissions are divided by 1.57 and 1.25 for biomass burning and anthropogenic emissions, respectively, to convert OM to OC prior to application of factors f_i in Table 3. The enthalpy of vaporization ΔH_{vap} is assumed to be 83 kJ mol^{-1} as in Pye and Seinfield (2010), but the model is not very sensitive to ΔH_{vap} for the two volatility species used in the condensed mechanism as the material represented by either species is firmly in one phase and far from the region where substantial fractions are in both phases.

The SAPRC-99 gas-phase chemistry leading to ozone formation in condensed 2-species VBS is exactly the same as detailed 9-species VBS. However, reactions and SOA yield leading to SI-SOA and V-SOA formation are different and are discussed in the following section.

ACPD
10, 30205–30277, 2010

2.2.2 SOA formation

2.2.2.1 SI-SOA

SI-SOA is formed by gas-phase oxidation of S/IVOC vapors represented the 2nd volatility species (C_{sat} of 10^5 µg m^{-3}), with each generation of oxidation moving material to the 1st volatility species, thus representing 7 orders of magnitude reduction in volatility. Also, the reaction rate with OH radical is reduced by a factor of 7 as compared to 9-species VBS approach (OH reaction rate of 0.57×10^{-11} molecule cm^{-3} s^{-1}). An addition of 50% oxygen mass is also assumed for the one generation of oxidation (instead of 15% in the 9-species VBS approach) following the discussions by Pye and Seinfield (2010).

Equations (1)–(4) are repeated within KPP for the 2-species VBS approach, but these equations are only written once resulting in oxidation of S/IVOC of species 2 on the left hand side to form SI-SOA represented by species 1 on the right hand side. The large addition of oxygen and reduction of volatility in one oxidation step is not meant to represent a physical process, but rather to parameterize the average effect of the more complex real processes, as the 7 times slower OH reaction rate makes up for the large changes, bringing predictions of SI-SOA in the 2-species VBS closer to 9-species VBS as shown later.

2.2.2.2 V-SOA

V-SOA formation is represented using fixed 1-product yields of these species. In the 4-product basis set for V-SOA as described by Tsimpidi et al. (2010), the lowest volatility species has a C^* of 1 µg m^{-3}. For consistency, the volatility of 1-product V-SOA is assumed to have a C^* of 1 µg m^{-3} at 298 K. The NO_x dependent 1-product mass yields for traditional anthropogenic and biogenic V-SOA precursors are given in Table 5. The SOA yields for alkane and olefin species are chosen to be equal to the yields corresponding to species with C^* of 1 µg m^{-3} in the 4-product VBS from Tsimpidi

ACPD
10, 30205–30277, 2010

et al. (2010). Yields for ARO1 and ARO2 are assumed to be equal to toluene and m-xylene SOA yields respectively following Ng et al. (2007b). These yields are chosen to be higher than respective ARO1 and ARO2 yields corresponding to C^* of 1 µg m^{-3} in Table 3. Yields for TERP and SESQ species are assumed to be equal to α-pinene and aromadendrene respectively (Ng et al., 2007a). All yields are chosen at lowest ΔM_0 values measured during the experiments to ensure atmospherically relevant conditions. The traditional A-V-SOA and B-V-SOA predicted from the 4-species formulation shown in Table 3 were found to be similar to the 1-species formulation shown in Table 5. Also B-V-SOA predicted by both formulations (Tables 3 and 5) is found to be factor of 5 lower as compared to the previous study by Hodzic et al. (2009) as shown later, mainly due to lower biogenic emissions in this work.

2.3 Dry and wet deposition

Dry deposition for all gas-phase SOA precursor species is calculated using the resistance model of Wesley (1989) assuming a Henry's law constant of 2700 M atm^{-1} which is used for species such as cresol and condensable organic gases as documented in CAMx user's guide (Environ, 2009). Dry deposition of OA is treated within MOSAIC similar to inorganic aerosols. Wet deposition is neglected in present work. Cloud-aerosol interactions, including wet removal, for all aerosols are not accounted for because the first two weeks of the MILAGRO campaign were mostly cloud free (Fast et al., 2007). Periods of afternoon convection and scattered precipitation did occur during the last week of the field campaign, but previous simulations using WRF-Chem by Fast et al. (2009) found that the amount of aerosols removed by the wet deposition during that period was relatively small. Also, the computational burden of handling the cloud processes would be unnecessarily excessive.

ACPD
10, 30205–30277, 2010

2.4 Modeling runs

A nested grid configuration with an outer grid using $12 \times 12\,km^2$ grid spacing and an inner grid using $3 \times 3\,km^2$ grid spacing is used to model the Mexico City region. For both detailed and condensed mechanisms, all OA species including freshly emitted POA and SOA are assumed to form an ideal solution. The total OA within the modeling domain is calculated as the sum of POA, SOA, and a small amount ($0.1–0.3\,\mu g\,m^{-3}$) of background OA coming from boundary conditions obtained from MOZART global simulations of trace gases and aerosols (Emmons et al., 2010). Initial and boundary condition for all newly added VBS OA species is assumed to be zero. Three modeling cases were carried out. The 9-species VBS was run for two anthropogenic S/IVOC emissions cases: (1) default emissions from 2006 inventory, (2) twice the amount of default S/IVOC emissions as compared to (1). S/IVOC emissions from biomass burning are assumed to be identical in both cases. The reasoning behind these runs is that default emissions from (1) using the 2006 MCMA inventory significantly under-predicted HOA as compared to AMS measurements. Using twice the amount of S/IVOC emissions allows us to study the sensitivity of HOA and SOA to anthropogenic emissions. In the third model Case, the condensed 2-species VBS mechanism was run with S/IVOC emissions equal to Case (2) above. Thus comparison of Cases (2) and (3) enables us to evaluate the condensed mechanism against the detailed 9-species VBS mechanism. The condensed mechanism predicts the same information as the 9-species VBS including source-resolved POA and SOA mass concentrations, and evolution of O:C ratios using the 4-species sectional representation for aerosols.

For comparison with measurements, model predictions are spatially and temporally interpolated to the location of the measurement for both aircraft flights and ground site data using the Aerosol Modeling Testbed Toolkit developed for WRF (Fast, 2011). Ground measurements are compared with the lowest level in the model ($\Delta z \sim 25\,m$). Comparisons between measurements and model predictions are done at local ambient conditions of pressure and temperature for both ground sites and aircraft flights. Also,

ACPD
10, 30205–30277, 2010

all WRF-Chem results are extracted for the inner grid using $3 \times 3\,km^2$ grid spacing. Spatial maps shown in the present study (for e.g. Fig. 1) represent the part of modeling domain where the nested grid configuration was used. The larger $12 \times 12\,km^2$ grid spacing modeling domain is shown in previous studies e.g. Fast et al. (2007).

2.4.1 Enhancement ratios with respect to CO

OA concentrations in the atmosphere evolve with changing boundary layer height, emissions and chemistry. On regional timescales, CO is a relatively inert tracer for dilution due to changes in boundary layer height and transport. To account for effects of dilution and transport, most of the model-measurement comparisons for OA in this work are discussed in terms of corresponding enhancement ratios with respect to CO. Measured and simulated values of OA components are normalized with respect to corresponding ΔCO ($CO\text{-}CO_{background}$) values. Fast et al. (2009) showed that simulated CO from WRF-Chem compared reasonably well with surface and aircraft observations. Background CO values of 50 ppb are assumed in this study. A previous study looked at uncertainty introduced by use of background CO values ranging 50–150 ppb (de Gouw et al., 2009). In the present study, a lower background CO is used (as compared to 100 ppb in other studies) to increase the number of non-negative ΔCO normalized OA concentrations during flight tracks. Since both measurements and model are normalized in a similar way, choice of a given background CO concentration does not affect the main conclusions in this paper.

3 Results and discussions

In this section, highly time-resolved AMS measurements at two surface sites (T0 and T1) and several aircraft flights (8 G-1 flight tracks and 2 C-130 flight tracks) are used to examine model performance within and around Mexico City. Predicted organic aerosols are evaluated with respect to both total OA and components of OA derived from PMF analysis: HOA, OOA and BBOA.

ACPD
10, 30205–30277, 2010

3.1 Spatial distributions of SOA

Figure 1 shows spatial distributions of 24-day average total SOA surface concentrations during 6–30 March 2006, as predicted by the three modeling cases. SOA predictions from 9-species VBS and condensed 2-species VBS cases (Cases 2 and 3) are very similar throughout the modeling domain. In comparison, Case 1 with half the anthropogenic S/IVOC emissions predicts lower SOA formation as expected, due to smaller amounts of S/IVOC precursors as compared to the other two cases.

Figure 2 shows the 24-day average contributions of various SOA components as a percentage of TOTOA for Case 2. As shown in Fig. 2a, A-SI-SOA contributes 20–30% to TOTOA at T0 site located within Mexico City. As the S/IVOC precursors move downwind and undergo multiple generations of oxidation chemistry, A-SI-SOA is dominant and contributes 50–70% to TOTOA. BB-SI-SOA forms the second major component contributing 10–30% to TOTOA as shown in Fig. 2b. The upper-right corner of Fig. 2b shows dominant BB-SI-SOA contribution in a part of Gulf of Mexico, but 24-day average absolute concentrations of BB-SI-SOA ranged 0.6–0.8 $\mu g\,m^{-3}$ in that region, and were less than 1 $\mu g\,m^{-3}$ over the entire Gulf of Mexico. In comparison, higher BB-SI-SOA concentrations ranging 1.7–2.0 $\mu g\,m^{-3}$ are observed over land and areas surrounding Mexico City (at T0 and T1 sites not shown here). Figure 2c and 2d shows that both traditional SOA components (B-V-SOA and A-V-SOA) contribute a much lower fraction (2–5%) to total OA. B-V-SOA is higher in areas where biogenic emissions are higher, whereas A-V-SOA is highest within the city and decreases downwind. B-V-SOA predictions in this work are a factor of 5 lower at T0 and T1 sites as compared to previous estimates by Hodzic et al. (2009) using CHIMERE model, and SOA-tracer based estimates by Stone et al. (2010). The low B-V-SOA predictions are chiefly due to factor of 5 lower isoprene emissions in WRF-Chem compared to CHIMERE model, as discussed earlier. The decrease in A-V-SOA is in contrast to the increase in A-SI-SOA downwind from Mexico City. This decrease is due to the fact that in the present formulation, A-V-SOA is formed only by first generation products of V-SOA precursors emitted close to

ACPD
10, 30205–30277, 2010

the city, while A-SI-SOA formation continues downwind due to multiple generations of chemistry.

3.2 Evaluation of OA components at T0 site

The T0 site is situated within the center of Mexico City, representing an area dominated by urban emissions. In WRF-Chem oxidation by OH radicals leads to SOA formation, so accurate representation of OH radical concentrations is necessary. As shown in the supporting information Fig. S1, WRF-Chem under-predicts OH concentration peak at day-time by a factor of 2 as compared to observations at the T0 site (Dusanter et al., 2009), but reproduces the timing of the OH peak. Also, WRF-Chem predicts near-zero OH concentrations during night-time, while measurements show higher concentrations but effects of low OH concentrations observed during night-time (order of magnitude lower than day-time) on SOA formation is expected to be small.

CO measurements are not available at T0 site; however, CO measurements from a nearby operational monitoring site are used to normalize observed OA values. Model $\sum \mathrm{POA(a)}_{i,\mathrm{antrhopogenic},x,n}$ is compared to PMF HOA factor, $\sum \mathrm{SI\text{-}SOA(a)}_{i,e,x,n} + \sum \mathrm{V\text{-}SOA(a)}_{i,e,x,n}$ is compared to PMF OOA, $\sum \mathrm{POA(a)}_{i,\mathrm{biomass-burning},x,n}$ is compared to PMF BBOA, and total simulated $PM_{2.5}$ OA is compared to measured total OA from PMF. Figure 3 compares observed and simulated enhancement ratios of HOA and OOA with respect to ΔCO at the T0 site.

3.2.1 HOA

Models reproduce observed diurnal variations of HOA/ΔCO peaking in the early morning rush hour period due to traffic emissions as shown in Fig. 3a. However, all 3 modeling cases under-predict the observed peaks in HOA enhancement ratios relative to CO. Figure 3c shows that on an average across all days, the default emissions (Case 1) under-predicts morning HOA peak by a factor of 3, implying problems with the 2006 emissions inventory. Case 2 (9-species VBS) and Case 3 (2-species VBS) with

ACPD
10, 30205–30277, 2010

twice the anthropogenic S/IVOC emissions better represent traffic emissions. HOA peak from 9-species VBS are 20–25% higher than 2-species VBS during early morning. The difference is related to the volatility distribution of SVOC emissions, as the 9-species VBS allows dynamic gas-particle partitioning using a globally non-volatile fraction of 22% as described earlier, while the 2-species VBS assumes that a constant fraction (one-third) of the SVOC emissions are HOA at all times. For example, if the total SVOC+IVOC concentration is 75 $\mu g\,m^{-3}$ at 20 °C, then volatility distribution from Cases 2 and 3 predicts POA concentrations of 8.6 and 10 $\mu g\,m^{-3}$, respectively. It is also interesting to note that while HOA/ΔCO peaks early close to 05:00 LT as shown in Fig. 3c, absolute HOA surface concentration peaks later in the morning at 07:00 LT as shown in Fig. 4c. The difference in timing of the two peaks is related to diurnal variation of CO concentrations.

3.2.2 OOA

Figure 3b shows that after 18 March, OOA enhancement ratios are under-predicted by all modeling cases. The average diurnal plot in Fig. 3d shows that all model cases reproduce the two observed peaks in OOA enhancement ratios. The early morning peak close to 04:00 local time is rather unexpected since photochemistry is not active to cause SOA production. Model peaks do not result from night-time chemistry with O_3 or NO_3 radicals, since night-time chemistry leading to SOA formation is not represented in WRF-Chem. The early morning peak in OOA/ΔCO in both PMF and WRF-Chem predictions shown in Fig. 3d is not due to formation of fresh SOA within the boundary layer. Also, Fig. 4d shows that total column burden of predicted SOA at the T0 site decreases during night-time till 08:00 LT as discussed in the following section. This morning peak is caused due to relatively sharper drop in ΔCO during this time. Interpretation of night-time CO data is more complicated as errors are amplified by shallow boundary layer during night, and mixing of residual layer above the boundary layer makes ΔCO normalized OA values more uncertain during night as compared to day-time.

ACPD
10, 30205–30277, 2010

Absolute values of surface SOA concentrations predicted by WRF-Chem (shown in Fig. 4c) are constant throughout the day due to compensating effects of dilution by growth of boundary layer and photochemistry as day progresses. When OOA is normalized to ΔCO to account for effects of dilution as shown in Fig. 3d, the afternoon peak due to photochemical SOA production is easily seen. PMF OOA peaks later in the afternoon with twice the magnitude of the early morning peak, which is not captured by Case 2, consistent with the underprediction of SOA/ΔCO in Fig. 3d. The timing of this peak is reproduced by the 3 modeling cases. Among the 3 modeling cases, the 2-species VBS (Case 3) is closest to PMF OOA, predicting two times higher afternoon peak as compared to morning. The differences between 9-species and 2-species VBS are due to volatility distribution of SOA, as the 2-species VBS causes all SOA formed to be almost non-volatile at ambient conditions (C^* of $10^{-2}\,\mu g\,m^{-3}$), while the 9-species VBS allows evaporation of SOA with dilution as the boundary layer grows. The default emission (Case 1) under-predicts the afternoon OOA peak by a factor of 2, implying that SOA precursor emissions are under-represented in the default inventory. Another possibility might be that chemistry is not adequately represented; however, both Case 2 and Case 3 show closer predictions with the same chemistry, and also SOA enhancement ratios are over-predicted downwind by all three cases as seen by aircraft flights discussed later. Hence within the existing modeling framework, the under-predictions of HOA and OOA using default emissions (Case 1) seems to be a result of lower emissions rather than chemistry. Dzepina et al. (2009) in a box modeling study derived HOA and S/IVOC from observations, rather than the emissions inventory, and observed better closure between modeled SOA and OOA observations. Aiken et al. (2009) concluded that total primary PM (not the same as POA) was underestimated by about a factor of 4 with respect to the 2006 emissions inventory, therefore it is possible that an underestimation of urban POA emissions remains in Case 2, leading to the observed discrepancy. Also, the 2006 biomass burning emissions inventory for Mexico City under-predicts BBOA as compared to PMF BBOA (not shown). Missing SOA from biomass burning precursors may also be responsible for model-measurement

ACPD
10, 30205–30277, 2010

differences in OOA, although the BBOA under-prediction is stronger during the early morning (not shown), and the low levels of the biomass burning tracer acetonitrile at T0 during afternoons (Aiken et al., 2010) make this possibility less likely.

3.2.3 Vertical profile, surface concentration and column burden

In addition to surface concentrations, it is also useful to look at vertical concentration profile and total column integrated burden of various OA components. Surface concentrations of pollutants are monitored for their health impacts, while vertical concentration profile and total column burden is important for climate effects.

Figure 4a shows the vertical distribution of HOA, SOA, BBOA and TOTOA concentrations, while Fig. 4b shows ratio of OA components to TOTOA with height above ground level (a.g.l.) at the T0 site. HOA concentrations are maximum at the surface (48% of TOTOA as shown in Fig. 4b) and decrease with increasing a.g.l. SOA concentration is comparable to HOA at the surface, but decreases much slower as compared to HOA at higher levels. Figure 4b shows that ratio of SOA/TOTOA increases from 0.5 near the surface to 0.75 at 1–4 km a.g.l. height. Continued photochemical oxidation of SOA precursors in the atmosphere causes SOA to be dominant component of TOTOA above the surface even at highly urbanized T0 site as shown in Fig. 4b. Thus model predictions imply that SOA is the most important component of OA in the atmosphere affecting both human health and climate. The ubiquity and dominance of SOA in the atmosphere is also implied by PMF analysis of AMS measurements (Zhang et al., 2007). The fractional importance of BBOA increases with height from 4% near the surface to 12% at 3 km a.g.l. as shown in Fig. 4b. The vertical distribution of BBOA emissions in WRF-Chem is based on the fire emission locations in the hills and mountains surrounding Mexico City, as well as mixing of smoke in the boundary layer before it is transported into Mexico City. Previous aircraft measurements have also seen increasing BBOA with height in Mexico City (Aiken et al., 2010; Crounse et al., 2009).

Figure 4d shows diurnal variation of total column integrated burden (mg m^{-2}) of OA components in the atmosphere. Solid lines in the figure represent results from Case 2

ACPD
10, 30205–30277, 2010

in present study, while dashed lines represent estimations from previous work by Aiken et al. (2010). The SOA burden decreases during night-time, but increases due to photochemistry in the day peaking at 16:00–17:00 LT. The magnitude and timing of daytime peak in SOA burden is comparable to the previous estimates by Aiken et al. (2010), which calculated the column burdens by multiplying surface concentrations with boundary layer depths assuming constant concentration across depth of boundary layer. Aiken et al. (2010) neglected species present above boundary layer in the morning. In the present study, column burden is calculated by integrating vertical concentration profile of OA components adding species present within and above the boundary layer till the top of modeling domain as predicted by WRF-Chem. SOA estimated by Aiken et al. (2010) in the night-time and early morning till 08:00 LT are factor of 4–9 lower than present study as shown in Fig. 4d. There is good agreement for the middle of the day when the convective boundary layer is deep, but the column burden is strongly underestimated using the method of Aiken et al. (2010) in the nighttime and early morning when the boundary layer is shallow, when there may be substantial OA in the residual layer above the boundary layer.

It is also instructive to compare diurnal variations of total column burden vs. surface concentration of various OA components as shown in Fig. 4c and d. Surface concentration shown in Fig. 4c changes due to evolution of boundary layer as the day progresses, but the total column integrated burden (shown in Fig. 4d) is not influenced by vertical dilution due to changing boundary layer. Surface SOA concentrations do not indicate significant diurnal variation due to opposing effects of dilution and photochemistry, but total SOA burden shows a strong diurnal variation due to photochemistry. Also HOA surface concentration peaks at 07:00 LT, but column burden of HOA is nearly constant throughout the day. BBOA surface concentrations and column burden both show similar diurnal variations with peaks at 18:00 LT due to relatively uniform vertical distribution of BBOA shown in Fig. 4a and b. Total OA surface concentrations and column burden follow corresponding diurnal variations of SOA.

ACPD
10, 30205–30277, 2010

3.2.4 O:C ratio

The evolution of the carbon and oxygen parts of SI-SOA are explicitly tracked, making it possible to calculate temporal and spatial variations in elemental O:C ratios in the aerosol phase. Figure 5a compares measured and simulated (Cases 1 and 2) temporal variation of O:C ratios at the T0 site, while Fig. 5b looks at 24-day average spatial variation of elemental O:C ratios predicted by Case 2. In this study, two oxygen atoms are added per generation of oxidation of S/IVOC precursors as discussed earlier. Figure 5a shows that both modeling cases reproduce the temporal variations of O:C ratios, but the magnitude is under-predicted at the T0 site. Case 1 is closest to AMS measurements predicting higher elemental O:C ratios as compared to Case 2. O:C ratios decrease as fresh reduced primary organic emissions are added every hour in the model, but increase as photochemistry causes SOA formation with addition of oxygen. Case 1 has half of the fresh reduced anthropogenic emissions as compared to Case 2, resulting in higher O:C ratios.

Case 3 (2-species VBS not shown) predicts very similar O:C ratios as Case 2 at T0 site. The agreement in O:C ratios between Case 2 and Case 3 over the city is very interesting. Case 2 represents 9-species VBS with 15% added oxygen mass per generation of oxidation, while Case 3 represent 2-species VBS with 50% added oxygen mass, and 7 times slower chemistry as compared to Case 2. Figure 5b shows that predicted 24-day average O:C ratios varies spatially ranging from a high of 0.3 at T0 site increasing to 0.6 further downwind, and could be as high as 0.7 over the Gulf of Mexico representing highly oxygenated organic material. In comparison, Hodzic et al. (2010a) and Dzepina et al. (2010) predicted much smaller O:C ratios ranging 0.14–0.24 over the Mexico City domain using the ROB approach adding one oxygen atom per generation of oxidation following Robinson et al. (2007), but better predicted the O:C ratios both within the city and downwind using the GRI approach in which the added oxygen mass was 40% and the chemistry was 2 times slower than in our simulation.

ACPD
10, 30205–30277, 2010

Figure 5c and 5d compare AMS O:C ratios to WRF-Chem simulations along C-130 flight tracks on 10 March (a high biomass burning day) and 29 (a low biomass burning day), respectively. A portion of the C-130 flight transects were located further downwind of Mexico City as discussed later. All 3 model Cases reproduce variations in measured AMS O:C ratios on 10 March reasonably well; but simulations under-predict peaks in O:C ratios, specially at downwind locations. The two large peaks in O:C ratios predicted by Case 1 and Case 2 in Fig. 5c are during lowest OA predictions events chiefly dominated by SOA. On 29 March, WRF-Chem simulations consistently under-predict O:C ratios as compared to measurements (shown in Fig. 5d). Most of the simulated values vary around 0.5, while AMS measured O:C ratios as high as 0.8 downwind of Mexico City on this day. It is important to note that the 2-species VBS (Case 3) predicts lower O:C ratios than 9-species VBS (Case 2) over downwind locations on this day; however the differences between these cases are less than 25%. All 3 modeling cases show very similar temporal variations in O:C ratios, which is expected since temporal variations in emissions, deposition, meteorology, and chemistry are similar within WRF-Chem for all runs.

Results from both this study and previous studies show a strong sensitivity of O:C ratios to the assumed oxygen added per generation of oxidation and point towards a need for additional experimental validation. Also fragmentation reactions which could cause an increase in O:C ratios (Kroll et al., 2009) need to be included in future parameterizations. Improving emission estimates for e.g. increasing biomass burning emissions would also help to increase O:C ratio predictions bringing them closer to measurements. Accurate predictions of O:C ratios are important to better understand the resulting effects on direct and indirect radiative forcing of climate by relating aerosol optical properties and CCN activation as function of chemical processing of OA in the atmosphere (Jimenez et al., 2009).

ACPD
10, 30205–30277, 2010

3.3 Evaluation of OA components at T1 site

The T1 site is located at the northern edge of the city. As discussed in Fast et al. (2009), the present WRF-Chem setup uses $3 \times 3\,km^2$ grid spacing which may not be enough to represent the strong spatial gradients of emissions in this region. Figure 6a–d show averaged diurnal variations of total OA, HOA, OOA and BBOA enhancement ratios with respect to CO, respectively. As shown in Fig. 6b, Case 1 with default emissions better represents HOA at the T1 site, while the other two modeling cases over-predict the early morning HOA peak by a more than a factor of 2. Figure 6c shows that the late afternoon peak in SOA due to photochemical production is over-predicted by Case 2 and Case 3, while Case 1 with lower S/IVOC precursor emissions represents this peak well. Some of this over-prediction in SOA/ΔCO may also be due to uncertainties in chemistry parameterization producing too much SI-SOA downwind of the city center. All three modeling Cases over-predict early morning PMF OOA peak. Also since emissions are more processed at the downwind T1 site as compared to the T0 site, OOA/ΔCO are expected to be higher at T1 as compared to T0. Greater differences in OOA/ΔCO in the afternoon peaks are predicted by all 3 modeling cases (factor of 2 higher at T1 compared to T0 as shown in Figs. 3d and 6c), as compared to measurements which show 25% higher OOA/ΔCO afternoon peak at T1 as compared to T0. Measured and simulated BBOA concentrations are lower as compared to HOA and OOA at the T1 site as shown in Fig. 6d. The late afternoon BBOA peak is under-predicted by about a factor of 3 as compared to measurements, pointing to limitations in biomass burning emission inventory.

Overall, the default emissions inventory (Case 1) represents surface level HOA and OOA at the T1 site better than at the T0 site, suggesting that spatial distribution of OA precursor emissions needs to be revised in the 2006 emissions inventory. Consistent with trends in HOA and OOA, total OA is over-predicted by Case 2 and Case 3, while Case 1 shows the best predictions at the T1 site as compared to observations. It is useful to note that at the T0 site, Case 1 under-predicts total OA (average diurnal variation not shown) by at least a factor of 2.

ACPD
10, 30205–30277, 2010

3.4 Evaluation of OA at remote sites

It is also instructive to evaluate OA variations at sites located farther from the city. In this section we look at two remote sites: T2 and Altzomoni. The T2 site was located 35 km to the north north-east of T1 at Rancho la Bisnaga, at an altitude of 2542 m. There are few significant anthropogenic emission sources between T1 and T2, and somewhat higher concentrations of OC and EC were found at T2 during periods of southwesterly winds (Doran, 2007). The mountain site of Altzomoni was located 60 km south-east of Mexico City at an altitude of 4010 m (Baumgardner et al., 2009). The Altzomoni site is generally above regional mixed layer from late evening until late morning. The T2 and Altzomoni sites are indicated in Fig. 1a.

Using thermal-optical OC/EC analyzer, Doran et al. (2007) reported organic carbon (OC) concentrations at T2 site, which are converted to TOTOA using an OM/OC ratio of 1.4. Figure 7a and b compare 24-day average diurnal variations of TOTOA and SOA from the 3 modeling cases. AMS OOA is not available for comparison to model predictions in Fig. 7b. Figure 7a shows that Case 2 and Case 3 reasonably predict concentrations of TOTOA. Also no strong diurnal variation in absolute TOTOA concentrations at T2 site is apparent. A comparison of Fig. 7a and b shows that model predictions indicate SOA to be dominant component of TOTOA at this site throughout the day.

Figure 7c and d show 24-day average diurnal variations of TOTOA and SOA, respectively, at the high altitude Altzomoni site. The top of the mixed layer reaches the altitude of Altzomoni at about 11:00–12:00 LT and remains above this altitude until after 20:00 LT. All modeling scenarios reproduce magnitude and diurnal variation of measured TOTOA concentrations (using AMS) as shown in Fig. 7c. As expected, both TOTOA and SOA concentrations increase at this site after 11:00 LT as the top of the mixed layer reaches the altitude of 4 km. As with the T2 site, most of the simulated TOTOA at the Altzomoni site is comprised of SOA.

ACPD
10, 30205–30277, 2010

3.5 Evaluation of OA components aloft

AMS measurements aloft are available from G-1 (Kleinman et al., 2008) and C-130 (DeCarlo et al., 2008) aircraft flight transects. The two aircrafts made several transects on different days flying above the center of Mexico City and downwind. This data is valuable to study time evolution and growth of organic aerosols due to gas-particle partitioning and photochemical aging of organics in the atmosphere. In this study, high time-resolution AMS PMF data (10-s data) from eight G-1 flights including 6a, 7a, 15a, 18a, 19a, 20a, 20b, 22a (a and b refer to morning and afternoon flights), and two C-130 flights (on 10 and 29 March) are used to evaluate simulated OA. The G-1 aircraft flew over Mexico City and up to 50 km northeast of the city, whereas the C-130 also flew further downwind over the Gulf of Mexico.

Figure 8 compares WRF-Chem output for Case 2 vs. PMF results from the AMS aboard the G-1 and C-130 flights. Results are shown as scatter plots of mass concentrations vs. CO mixing ratios. Higher CO mixing ratios (≥500 ppbv) are generally associated with the city center or within fire plumes, while lower CO mixing ratios represent instances when aircrafts were flying farther downwind. Figure 8a and c shows that HOA is significantly under-predicted aloft over Mexico City and immediately downwind of city. HOA predictions improve at farther downwind locations (CO mixing ratios lower than 250 ppb). SOA predictions in Fig. 8b and d show the reverse trend as compared to HOA. SOA predictions are much better over the city and immediate downwind locations, but SOA is over-predicted as compared to AMS OOA at more remote downwind locations. The two branches appearing in HOA and SOA scatter plots for Case 2 predictions in Fig. 8 are interesting. In Fig. 8b, the first branch showing high SOA at low CO concentrations (below 250 ppb CO) comes mainly from higher anthropogenic A-SI-SOA contributions for five G-1 flight paths. Higher BB-SI-SOA contributed to higher SOA at downwind locations for the remaining three G-1 flight paths on 15, 18 and 19 March at downwind locations as compared to within the city. In Fig. 8d, some of the highest SOA predictions at downwind locations are caused by high A-SI-SOA on

ACPD
10, 30205–30277, 2010

10 March 2006. High BB-SI-SOA also contributes to downwind SOA on both 10 and 29 March 2006. Significant contributions of A-SI-SOA downwind are also consistent with the high downwind HOA branch from model predictions appearing in both Fig. 8a and c. In comparison to model predictions, PMF HOA shows more scatter (Fig. 8a and c). The model has difficulty representing this scatter, thus highlighting significant uncertainties in representation of spatial and temporal variation of emission sources in the 2006 MCMA inventory. This inconsistency related to uncertainties in emissions inventory has also been shown in previous work by Fast et al. (2009).

Percentiles are used to compare the range of PMF factor enhancement ratios relative to CO and WRF-Chem predictions along individual G-1 and C-130 flights as shown in Fig. 9. On all days except the C-130 flight track on 29 March, median predictions of HOA/ΔCO are lower than that derived from PMF as shown in Fig. 9a. PMF HOA/ΔCO ratios also show greater variability on any given day as compared to predictions. Part of the variability in PMF HOA may arise due to the fact that PMF of unit resolution data used for the G-1 aircraft, has difficulty separating contributions of HOA and BBOA (Aiken et al., 2009). C-130 data utilize high-resolution AMS data, which is much better able to separate HOA and BBOA components. But as discussed earlier, significant spatial and temporal variation of emissions also causes higher variability in PMF HOA/ΔCO ratios which is not captured by 2006 MCMA emissions inventory used in this work.

Almost an opposite trend is seen for OOA enhancement ratio comparisons in Fig. 9b. On most days except the mornings of 6, 7, and 20 March, the model over-predicts median SOA/ΔCO ratios as compared to corresponding PMF OOA/ΔCO ratios. In addition, the predictions show greater variability as compared to PMF observations. The greatest predicted variability in the simulations is seen for the G-1 flight on morning of 22 March and the C-130 flight on 10 March. 10 March was a high biomass burning day with several large fires within 60 km of Mexico City. Biomass burning contributions to SI-SOA on this day were similar to anthropogenic SI-SOA contributions (as shown in Fig. 10f discussed later).

ACPD
10, 30205–30277, 2010

Figure 9 also shows that magnitude and variability of all OA component enhancement ratios (HOA/ΔCO, OOA/ΔCO and BBOA/ΔCO) predicted by 9-species VBS and 2-species VBS (Case 2 and Case 3, respectively) are very similar across all 10 individual flight tracks, providing evidence of the ability of 2-species VBS approach to represent OA components aloft both over the city and downwind. As expected, HOA and SOA predictions for Case 1 are lower than other 2 modeling cases due to half the anthropogenic S/IVOC emissions as discussed earlier and shown in Fig. 9a and 9b, respectively. Figure 9c shows that predicted BBOA/ΔCO ratios across most flight tracks (especially evident on high biomass burning days, such as 10 March) are too low, pointing to significant uncertainties and missing biomass burning smoke emissions in the inventory used here. Total OA/ΔCO ratios are generally under-predicted except for the last three flights to the right, as shown in Fig. 9d; however, there are compensating errors due to models under-predicting HOA and BBOA, and over-predicting OOA as compared to AMS data. Hence, it is extremely important to look at individual OA components such as HOA, OOA and BBOA to understand how total OA evolves in the atmosphere.

It is also instructive to look more closely at individual flights paths. Figures 10 and 11 compare WRF-Chem outputs to highly time resolved AMS data for OA components along the C-130 transect on 10 March and the G-1 transect on 15 March, respectively. On 10 March, MODIS detected several large fires within 60 km of Mexico City, thus it was a high biomass-burning day. 15 March was a day with relatively low biomass burning. Both WRF-Chem and AMS data are averaged to 1 min. time intervals to reduce high-frequency variability and ease visual comparison.

3.5.1 C-130 flight on 10 March

On the morning of 10 March 2006, the C-130 aircraft encountered a large number of biomass burning fires as detected by MODIS fire counts (Fast et al., 2009) as it flew from the Gulf of Mexico towards Mexico City. The aircraft sampled several downwind locations between Mexico City and Veracruz at (17:00–20:00 UTC or 11:00–14:00 local

ACPD
10, 30205–30277, 2010

time). Figure 10a shows that there may be small transport and dilution errors close to 18:30–19:00 UTC shown by difference in measured and simulated CO concentrations. When the aircraft flew close to the city over T0 and T1 sites (20.5–22 UTC or 14:30–16:00 local time), Figure 10a shows that CO is over-predicted somewhat by WRF-Chem as compared to observations; however, the temporal variations look consistent. The C-130 then flew back to Veracruz late in the afternoon.

Figure 10b shows that variations in total OA/ΔCO ratios are reasonably simulated over the city region. WRF-Chem slightly under-predicts total OA over the city as compared to AMS data. WRF-Chem over-predicts total OA by 50–100% as compared to AMS measurements when the aircraft flew downwind earlier during the day.

Figure 10c shows that HOA/ΔCO ratios are under-predicted by all modeling cases over the city by more than a factor of 3. But, OOA/ΔCO ratios over the city are predicted reasonably well (Fig. 10d). Some of the under-predicted HOA enhancement ratios are due to higher CO mixing ratios simulated by the model over the city. At most downwind locations CO predictions are closer to observations (Fig. 10a), both predicted and simulated HOA enhancement ratios are relatively low in magnitude, but OOA enhancement ratio is over-predicted by a factor of 2–3 as shown in Fig. 10d. Figure 10e shows that BBOA/ΔCO ratios are consistently under-predicted over the city and downwind locations pointing to problems in the biomass burning emissions inventory.

Figure 10f quantifies different SOA source-contributions in this study along the flight track using Case 2. These include V-SOA from traditional anthropogenic and biogenic precursors (A-V-SOA and B-V-SOA), and SI-SOA from S/IVOC precursor emissions related to anthropogenic and biomass burning emissions (A-SI-SOA and BB-SI-SOA, respectively). Both over the city and at downwind locations A-SI-SOA and BB-SI-SOA are equally important. Traditional A-V-SOA and B-V-SOA contributes a much smaller fraction to SOA both over city and downwind locations, and biomass burning and anthropogenic emissions (predominantly traffic emissions) are the two major SOA precursor sources within and around Mexico City region. Since BBOA is consistently under-predicted as shown in Fig. 10f, correcting for BBOA in WRF-Chem would increase

ACPD
10, 30205–30277, 2010

SOA contributions from biomass burning precursors in the current parameterization both over city and downwind locations. Because both total OA and SOA are over-predicted by all three modeling cases downwind of Mexico City (as shown in Fig. 10b and d), increasing the biomass burning precursors should be accompanied by decrease in biomass burning and/or anthropogenic S/IVOC precursors, or by a decrease in the efficiency of forming SI-SOA from S/IVOC. For example, the parameterization by Grieshop et al. (2009) did not include IVOCs for biomass burning based on their smog chamber experiments. Also, a decrease in anthropogenic SVOC emissions would lead to greater under-prediction in HOA/ΔCO ratio over the city. Other options include slowing down chemistry parameterizations, fragmentation reactions and increase in loss of S/IVOC precursors from dry deposition reducing SOA formation downwind of Mexico City. Total simulated OA/ΔCO ratios in Fig. 10b currently look better as compared to individual derived OA components due to compensating errors from simulated HOA and BBOA that are too low and OOA that is too high.

3.5.2 G-1 flight on 15 March

Another example is shown in terms of G-1 flight transects on the morning of 15 March in Fig. 11. This was a low biomass burning day as compared to 10 March. As shown in Fig. 11a, spatial variations of predicted CO are qualitatively similar to observations. The largest scatter in observed and simulated CO occurs over the city due to errors in timing and location of simulated plume (Fast et al., 2009).

Figure 11b shows that variations in total OA/ΔCO ratios are reasonably simulated by WRF-Chem over the city and nearby downwind locations. TOTOA is over-predicted at farther downwind locations mainly due to over-prediction in SOA consistent with C-130 flight comparisons in Fig. 9b.

As shown in Fig. 11c, simulated HOA is under-predicted over the city as compared to AMS HOA (during 17:00–17:30 UTC). Case 1 shows lower HOA as compared to other two cases due to lower anthropogenic S/IVOC emissions as discussed earlier. The consistent under-prediction in HOA enhancement ratios suggest revising SVOC

ACPD
10, 30205–30277, 2010

emissions or volatility distribution of emissions making higher fraction of SVOC emissions to be non-volatile under local ambient conditions.

Figure 11d shows that OOA is over-predicted by Case 2 and Case 3 over the city (having higher S/IVOC precursor emissions than Case 1). Between 16:00–16:30 UTC and 17:30–18:30 UTC the aircraft flew downwind over T1 and between Mexico City and Veracruz farther downwind. OOA is consistently over-predicted at downwind locations. Figure 11e also shows that BBOA is underpredicted on this day too by all modeling cases. It is also noteworthy that the Case 3 (2-species VBS) shows higher BBOA as compared to Case 2, primarily because 2-species VBS assumes 30% of the SVOC emissions from biomass burning to be non-volatile (as compared to 9% using the globally non-volatile fraction assumed by Case 2). In comparison, Case 2 and Case 3 assume an almost equal fraction of anthropogenic SVOCs to be non-volatile (23% and 30%, respectively).

Figure 11f shows SOA source-contributions using Case 2 along the flight transect. Over the city, A-SI-SOA is dominant contributor to SOA. At farther downwind locations, BB-SI-SOA starts playing a more important role consistent with conclusions from C-130 flight transect shown in Fig. 10f. Again both traditional A-V-SOA and B-V-SOA precursors contribute relatively low SOA mass as compared to S/IVOC precursors from anthropogenic and biomass burning emissions.

3.6 Non-fossil carbon fraction (f_{NF})

^{14}C measurements provide insights into relative contributions of fossil and modern carbon. These measurements provide another metric to evaluate predictions of source-oriented models such as WRF-Chem. Substantial amounts of non-fossil carbon as a fraction of total OC (f_{NF}) are observed in both urban locations such as Mexico City and in remote environments of the Northern Hemisphere throughout the year (Hodzic, 2010b). High values of f_{NF} observed in urban environments such as Mexico City during low biomass burning events points towards importance of representing non-fossil sources in emission inventories (Hodzic, 2010b). These sources include biogenic SOA,

ACPD
10, 30205–30277, 2010

primary biological particles (PBAP) and urban sources of non-fossil carbon such as food cooking, municipal trash burning, biofuel use, etc.

In this work f_{NF} is calculated using following assumptions: 20% of urban carbon (both primary and secondary) is non-fossil, 15% of biogenic SOA is PBAP consistent with results from Hodzic et al. (2010b), and both BBOA and SOA from biomass burning are non-fossil carbon sources. f_{NF} is not sensitive to dilution effects resulting from variation in boundary layer height as it is a ratio. Also f_{NF} does not depend on amount of oxygen added in the S/IVOC oxidation parameterization, as it is based on carbon fraction.

The non-fossil carbon fraction (f_{NF}) is found to range 0.37–0.67 at T0 and 0.50–0.86 at T1, with a substantial disagreement between two datasets collected by two different groups, which remains unresolved (Hodzic, 2010b). Figure 12 shows average diurnal variation of f_{NF} at the T0 and T1 sites, respectively, using Case 2 indicated by solid lines. The figure shows f_{NF} values ranging 0.26–0.40 and 0.34–0.43 at the T0 and T1 sites, respectively. Consistent with estimations by Hodzic et al. (2010b), f_{NF} values at T1 site are predicted to be higher by about 0.1 as compared to T0 site. Also, Fig. 12 indicates that f_{NF} values at both sites increases during the day after 08:00 LT with a peak value at 18:00 LT.

We note that B-V-SOA is too low in our model compared to previous studies as discussed earlier. So, f_{NF} is recalculated in our model by increasing B-V-SOA by a factor of 5 at the T0 and T1 sites as indicated by dashed lines in Fig. 12, keeping concentrations of all other OA components unaltered. Increasing B-V-SOA causes an increase in f_{NF} by 0.04 and 0.05 at the T0 and T1 sites, respectively, on an average.

It is also important to note that WRF-Chem predicts f_{NF} (average ~0.36 at T0 when biogenic SOA is corrected as above) which are slightly lower than the Aiken et al. (2010) f_{NF} dataset (average of 0.44), consistent with the results of Hodzic et al. (2010b). Since WRF-Chem has missing biomass emissions as well as especially early morning impacts which strongly affect the surface average concentrations (Aiken et al., 2010), increasing amount of biomass burning emissions would help to increase predicted values of f_{NF} bringing them into agreement to measurements, consistent with

ACPD
10, 30205–30277, 2010

the conclusions of Hodzic et al. (2010b). However, a separate dataset of f_{NF} from Marley et al. (2009) reports f_{NF} which is larger by about 0.15 compared to the Aiken et al. (2010) data, and the unexplained disagreement between these datasets limits our ability to make strong conclusions based on these comparisons. In addition, accurate quantification of OA and S/IVOC emissions and their non-fossil carbon fraction for anthropogenic trash burning observed within and around Mexico City, as well as for other urban emissions such as food cooking and biofuel use is also essential to better constrain model predictions of f_{NF}.

3.7 WRF-Chem vs. CHIMERE

Even though CHIMERE and WRF-Chem have differences in treatments of meteorology, chemistry, emissions, and coupling of meteorology with chemistry (offline versus online) they are widely used by different groups and it is instructive to compare OA predictions between the two models. WRF-Chem uses SAPRC-99 gas phase chemistry, whereas CHIMERE uses the MELCHIOR chemical mechanism. Details of SOA formation mechanism in CHIMERE are discussed by Hodzic et al. (2009) and Hodzic et al. (2010a). Since SI-SOA formation is primarily controlled by OH concentrations, inter-comparison of OH concentrations simulated by CHIMERE and WRF-Chem was done at the T0 site in Mexico City. Both models showed similar diurnal variations for OH, however, CHIMERE predicts higher average OH concentration as compared to WRF-Chem.

Also, in CHIMERE, dry deposition of all gaseous semi-volatile species is calculated similar to NO_2 (effective Henry's law constant of 0.01 M atm^{-1}), however, in WRF-Chem dry deposition is calculated using an effective Henry's law constant of 2700 M atm^{-1}. Hence dry deposition velocities of semi-volatile organic vapors in WRF-Chem are expected to be higher than CHIMERE. However, dry deposition velocities do not directly scale with effective Henry's law constant due to other factors as aerodynamic resistance, surface resistance, stomatal resistance and effect of reactivity on mesophyllic resistance (Bessagnet et al., 2010). Bessagnet et al. (2010) found that omitting dry

ACPD
10, 30205–30277, 2010

deposition of semivolatile species may overestimate SOA concentrations by as much as 50% especially during nighttime when relative humidity is high. Quantifying effects of dry deposition on SOA concentrations in WRF-Chem is a subject for further study.

Figures 13 and 14 compare total OA, HOA, SOA and BBOA predictions at the T0 and T1 sites respectively from CHIMERE (using the ROB approach) and WRF-Chem (Case 2). Temporally averaged simulated values from both the models are also indicated on each figure. The CHIMERE simulations of Hodzic et al. (2010a) used an older POA emissions inventory for Mexico City, while the current WRF-Chem predictions are from a recently revised inventory for Mexico City for 2006, with an additional doubling of the default anthropogenic S/IVOC emissions (Case 2 Cases) used for comparison. Older POA emissions used by Hodzic et al. (2010a) were greater than revised 2006 inventory used in this work by almost a factor of 2 at the T0 site, so Case 2 predictions of HOA are similar to Hodzic et al. (2010a). At the T0 site, the average predictions of total OA, HOA, SOA and BBOA are very similar in both models. This is encouraging as it implies that simulated OA components by the two models within Mexico City are of similar order. Differences in temporal variations between WRF-Chem and CHIMERE are also due to different treatments of meteorology. WRF-Chem using online meteorology as discussed earlier which is more useful for simulating event periods, while CHIMERE uses offline meteorology through MM5.

At the T1 site, shown in Fig. 14a, WRF-Chem predicts on average 25% higher total OA as compared to CHIMERE. Also, on an average WRF-Chem predicts lower HOA (10% lower) and higher SOA (50% higher) as compared to the CHIMERE model as shown in Fig. 14b and c, respectively. The S/IVOC emissions have had more time for multi-generational photochemistry leading to higher SOA/ΔCO ratios at the T1 site as compared to T0 site as discussed earlier. Differences in HOA are related to differences in emissions and spatial resolution of the model at the T1 site. As WRF-Chem assumes a minimum non-volatile fraction of 22% of SVOC emissions for anthropogenic emissions as compared to CHIMERE where the minimum non-volatile fraction is 9% (based on ROB approach), if emissions were same, WRF-Chem would predict higher

ACPD
10, 30205–30277, 2010

HOA as compared to CHIMERE. In contrast, lower HOA predictions from WRF-Chem indicate significant differences in emissions, transport and deposition between the two models. BBOA predictions are of the same order between CHIMERE and WRF-Chem as shown in Fig. 14d.

Figure 15 compares various SOA components between the two models at T1 site. Similar amounts of traditional A-V-SOA are predicted by both WRF-Chem and CHIMERE as shown in Fig. 15a. CHIMERE predicts 5 times higher B-V-SOA as compared to WRF-Chem shown in Fig. 15b as discussed earlier. Figure 15c and d shows that WRF-Chem predicts twice A-SI-SOA and 50% higher BB-SI-SOA as compared to CHIMERE on an average, with most of the higher predictions occurring after 24 March. Differences in meteorological treatments between the two models are partly responsible for differences in predicted OA. Higher SI-SOA predictions from WRF-Chem are also partially caused due to addition of 15% oxygen mass per generation of oxidation as compared to 7.5% added oxygen assumed by CHIMERE model. In addition, CHIMERE included treatment of precipitation and wet deposition after 24 March (Hodzic et al., 2010a), but amount of aerosols removed by wet deposition in CHIMERE was not quantified in that study. In contrast, wet deposition is excluded in WRF-Chem in the present study, as Fast et al. (2009) found that effects of wet deposition removal during that period was relatively small. Figure 15e shows that total SOA predicted by WRF-Chem is on average 50% higher as compared to CHIMERE, chiefly due to higher SI-SOA predictions by WRF-Chem.

4 Discussion

The VBS approach formulated by Robinson et al. (2007) is a very useful approach to represent varying gas-particle partitioning and multi-generational photochemical aging of a complex mixture of thousands of organic species in air-quality models. As shown in this study and several recent studies using this approach for Mexico City (Dzepina et al., 2009; Hodzic et al., 2010a; Tsimpidi et al., 2010), experiments constraining various

ACPD
10, 30205–30277, 2010

parameterizations related to emissions of S/IVOC precursors, volatility distribution, and chemistry including functionalization, fragmentation and oligomerization reactions are needed to improve predictions of both mass and oxidation state of OA in the atmosphere.

More research is needed to make sure that total OA is accurately predicted for the right reasons: i.e. all the components of OA including HOA, OOA, and BBOA need to be right as well. In addition, models also need to capture the evolution of O:C ratios of OA. AMS measurements during field experiments involving both ground and aircraft flights are valuable to help constrain parameters of the VBS approach. For example, we show that biomass burning emissions are consistently under-predicted by all model cases at both ground and aircraft locations pointing to a continued need to revise biomass burning emissions in and around Mexico City region. In addition, consistent under-prediction in HOA at T0 site within the city center and most aircraft flights aloft suggest that either primary anthropogenic SVOC emissions need to be increased or SVOC emissions have a higher non-volatile fraction than currently assumed. Also higher scatter in PMF HOA as compared to WRF-Chem predictions suggest that spatial and temporal variation of emissions in 2006 MCMA inventory need to be revised. Likewise, a consistent over-prediction in SOA at downwind locations is evident from most aircraft flights suggesting problems in chemistry parameterizations of S/IVOC precursors. The current parameterization adds 50–100% higher SOA mass as compared to estimates obtained from PMF analysis on AMS measurements. In addition, effect of loss mechanisms such as dry deposition of S/IVOC vapors downwind need to be quantified experimentally. Dry deposition of S/IVOC vapors downwind would reduce SOA formation bringing model predictions closer to AMS PMF analysis.

WRF-Chem predictions are close to one of the datasetes of non-fossil carbon (f_{NF}) reported for Mexico City, especially when the underpredictions in biogenic SOA and in BBOA are taken into account. However a substantial (~0.15) underprediction is observed when comparing with the other dataset (Marley et al., 2009), and the overall conclusion is unclear due to conflicting results from the two available experimental

ACPD
10, 30205–30277, 2010

datasets. A remaining under-prediction would reflect missing sources of non-fossil carbon such as additional biogenic SOA or biomass burning, as well as anthropogenic sources (trash burning, food cooking, biofuel use, etc.) in the emissions inventory. Non-fossil carbon emissions are highly uncertain due to challenges associated with identifying and quantifying their temporal and spatial distributions in the inventory.

OA and organic vapor measurements also need substantial improvements. Uncertainties in AMS measurements and subsequent PMF analysis also need to be better quantified. These uncertainties will vary spatially and temporally due to two factors. First, there were possible variations in collection efficiency among the different G-1 flights (Kleinman et al., 2008). These variations are inconsistent, however, with the good intercomparisons observed for the C-130 aircraft (DeCarlo et al., 2008) at the T0 site, which highlights the difficult of determining AMS collection efficiency from single instrument intercomparisons in the field. Second, PMF will have difficulty separating the contribution of different OA factors at locations and times when markers for different factors as HOA, OOA and BBOA co-vary in the atmosphere (which often occurred during MILAGRO), especially when unit-resolution data is used as for the G-1 aircraft and the T1 site (Aiken et al., 2009). Comparing PMF results to predictions from a source-oriented modeling approach such as WRF-Chem helps to identify the range of uncertainties in both source-oriented and PMF based approaches. At the same time, information from both types of approaches needs to be combined in a consistent manner to improve OA predictions in the atmosphere. In addition to improvements of the AMS and its analysis techniques, additional real-time instruments for OA characterization need to be developed and deployed, especially those that may have more detailed chemical markers for OA from different sources. Importantly, a measurement of total gas-phase species with some volatility and/or chemical resolution such as O:C (analogous to the AMS) is critically needed, as otherwise no comparison of predicted vs. measured bulk gas-phase species is possible, as in this study. Finally resolving the discrepancies between different non-fossil carbon measurements and performing those measurements with higher time resolution is important for better constraining

ACPD
10, 30205–30277, 2010

model results.

In addition, several other processes such as formation of SOA from volatile species as glyoxal, increase of biogenic SOA yields in presence of anthropogenic pollution for e.g. formation of organo-sulfates, organo-nitrates and esterification processes, and SOA formation in clouds, need to be studied and included in models.

5 Conclusion

The WRF-Chem community model has been revised to include SOA formation coupled to the inorganic MOSAIC code for the first time. Traditional V-SOA formation using NO_x-dependent yields from both traditional anthropogenic and biogenic VOC precursors are included. Non-traditional SOA formation from S/IVOC precursors is also implemented using the volatility basis-set approach following Robinson et al. (2007). In addition to 9-species VBS approach to model SI-SOA formation from S/IVOC precursor emissions, a highly condensed 2-species VBS approach is developed and tested with respect to similarity to the detailed 9-species VBS approach. AMS measurements at ground sites and aircraft sampling during MCMA 2006 is used to evaluate WRF-Chem simulations. Results show that 2-species VBS predictions of total OA, HOA, OOA and BBOA are similar to the 9-species VBS predictions (with same S/IVOC emissions) at both ground locations (T0 and T1 sites) and along 10 aircraft transects studied. In addition, the 2-species VBS also predicts evolution of O:C ratios similar to the 9-species VBS approach (within 25%). The simplified 2-species mechanism reduces the computational cost by a factor of 2 as compared to 9-species VBS. The computational expense can be reduced further if sources of organic aerosols and O:C ratios are not required. Thus the condensed 2-species mechanism is better suited for routine applications using computationally expensive models such as WRF-Chem running coupled cloud-aerosol-meteorology as well as global models. Validating the 2-species to the 9-species VBS predictions is an essential first step to using these highly condensed SOA mechanisms designed to represent the full complexity of information (both mass and

ACPD
10, 30205–30277, 2010

oxidation state of OA). WRF-Chem predictions are also compared to the CHIMERE model, and the two models show reasonable agreement of total OA (within 25%) at the T0 and T1 sites. Nevertheless, many uncertainties remain in both models as discussed earlier.

In the future, we plan to evaluate the impact of evolving mass and oxidation state (O:C ratio) of OA on aerosol optical properties (e.g. refractive index), hygroscopicity and CCN activity, and dry deposition of S/IVOC precursors varying with O:C ratios by means of WRF-Chem using more recent field and laboratory data. Additional well-coordinated field and laboratory measurements are needed to constrain these parameterizations as a function of photochemical aging of OA in the atmosphere.

Supplementary material related to this article is available online at: http://www.atmos-chem-phys-discuss.net/10/30205/2010/acpd-10-30205-2010-supplement.pdf.

Acknowledgements. We thank Miguel Zavala and Luisa Molina (Molina Center for Energy and the Environment) for providing the most recent MCMA emissions inventory, Christine Wiedinmyer (National Center for Atmospheric Research) for providing the biomass burning inventory, Sebastien Dusanter and Phil Stevens (Indiana Univ.) for OH data, Larry Kleinman (Brookhaven National Laboratory), Manjula Canagaratna (Aerodyne Research Inc.), Lizbeth Alexander (PNNL), and Peter DeCarlo, Allison Aiken, and Ingrid Ulbrich (Univ. of Colorado) for providing AMS data, and Georg Grell and Steven Peckham (NOAA/Earth System Research Laboratory) for their support of WRF-Chem. JLJ was supported by NOAA NA08OAR4310565. This research was supported by the US DOE's Atmospheric Sciences Program of the Office of Biological and Environmental Research (OBER) under Contract DE-AC06-76RLO 1830 at Pacific Northwest National Laboratory (PNNL). PNNL is operated for the US DOE by Battelle Memorial Institute.

ACPD
10, 30205–30277, 2010

References

Aiken, A. C., Decarlo, P. F., Kroll, J. H., Worsnop, D. R., Huffman, J. A., Docherty, K. S., Ulbrich, I. M., Mohr, C., Kimmel, J. R., Sueper, D., Sun, Y., Zhang, Q., Trimborn, A., Northway, M., Ziemann, P. J., Canagaratna, M. R., Onasch, T. B., Alfarra, M. R., Prevot, A. S. H., Dommen, J., Duplissy, J., Metzger, A., Baltensperger, U., and Jimenez, J. L.: O/C and OM/OC ratios of primary, secondary, and ambient organic aerosols with high-resolution time-of-flight aerosol mass spectrometry, Environ. Sci. Technol., 42, 4478–4485, doi:10.1021/es703009q, 2008.

Aiken, A. C., Salcedo, D., Cubison, M. J., Huffman, J. A., DeCarlo, P. F., Ulbrich, I. M., Docherty, K. S., Sueper, D., Kimmel, J. R., Worsnop, D. R., Trimborn, A., Northway, M., Stone, E. A., Schauer, J. J., Volkamer, R. M., Fortner, E., de Foy, B., Wang, J., Laskin, A., Shutthanandan, V., Zheng, J., Zhang, R., Gaffney, J., Marley, N. A., Paredes-Miranda, G., Arnott, W. P., Molina, L. T., Sosa, G., and Jimenez, J. L.: Mexico City aerosol analysis during MILAGRO using high resolution aerosol mass spectrometry at the urban supersite (T0) – Part 1: Fine particle composition and organic source apportionment, Atmos. Chem. Phys., 9, 6633–6653, doi:10.5194/acp-9-6633-2009, 2009.

Aiken, A. C., de Foy, B., Wiedinmyer, C., DeCarlo, P. F., Ulbrich, I. M., Wehrli, M. N., Szidat, S., Prevot, A. S. H., Noda, J., Wacker, L., Volkamer, R., Fortner, E., Wang, J., Laskin, A., Shutthanandan, V., Zheng, J., Zhang, R., Paredes-Miranda, G., Arnott, W. P., Molina, L. T., Sosa, G., Querol, X., and Jimenez, J. L.: Mexico city aerosol analysis during MILAGRO using high resolution aerosol mass spectrometry at the urban supersite (T0) – Part 2: Analysis of the biomass burning contribution and the non-fossil carbon fraction, Atmos. Chem. Phys., 10, 5315–5341, doi:10.5194/acp-10-5315-2010, 2010.

Andreae, M. O. and Merlet, P.: Emission of trace gases and aerosols from biomass burning, Global Biogeochem. Cycle, 15, 955–966, 2001.

Baumgardner, D., Grutter, M., Allan, J., Ochoa, C., Rappenglueck, B., Russell, L. M., and Arnott, P.: Physical and chemical properties of the regional mixed layer of Mexico's Megapolis, Atmos. Chem. Phys., 9, 5711–5727, doi:10.5194/acp-9-5711-2009, 2009.

Bessagnet, B., Seigneur, C., and Menut, L.: Impact of dry deposition of semi-volatile organic compounds on secondary organic aerosols, Atmos. Environ., 44, 1781–1787, doi:10.1016/j.atmosenv.2010.01.027, 2010.

Cappa, C. D. and Jimenez, J. L.: Quantitative estimates of the volatility of ambient organic aerosol, Atmos. Chem. Phys., 10, 5409–5424, doi:10.5194/acp-10-5409-2010, 2010.

ACPD
10, 30205–30277, 2010

Carlton, A. G., Bhave, P. V., Napelenok, S. L., Edney, E. O., Sarwar, G., Pinder, R. W., Pouliot, G. A., and Houyoux, M.: Model Representation of Secondary Organic Aerosol in CMAQv4.7, Environ. Sci. Technol., 44(22), 8553–8560, 2010.

Carter, W. P. L.: SAPRC-99 Mechanism Files and Associated Programs and Examples: http://www.cert.ucr.edu/carter/SAPRC99/, last updated 30 March 2010.

Crounse, J. D., DeCarlo, P. F., Blake, D. R., Emmons, L. K., Campos, T. L., Apel, E. C., Clarke, A. D., Weinheimer, A. J., McCabe, D. C., Yokelson, R. J., Jimenez, J. L., and Wennberg, P. O.: Biomass burning and urban air pollution over the Central Mexican Plateau, Atmos. Chem. Phys., 9, 4929–4944, doi:10.5194/acp-9-4929-2009, 2009.

Damian, V., Sandu, A., Damian, M., Potra, F., and Carmichael, G. R.: The kinetic preprocessor KPP – a software environment for solving chemical kinetics, Comput. Chem. Eng., 26, 1567–1579, 2002.

DeCarlo, P. F., Dunlea, E. J., Kimmel, J. R., Aiken, A. C., Sueper, D., Crounse, J., Wennberg, P. O., Emmons, L., Shinozuka, Y., Clarke, A., Zhou, J., Tomlinson, J., Collins, D. R., Knapp, D., Weinheimer, A. J., Montzka, D. D., Campos, T., and Jimenez, J. L.: Fast airborne aerosol size and chemistry measurements above Mexico City and Central Mexico during the MILAGRO campaign, Atmos. Chem. Phys., 8, 4027–4048, doi:10.5194/acp-8-4027-2008, 2008.

de Gouw, J. A., Middlebrook, A. M., Warneke, C., Goldan, P. D., Kuster, W. C., Roberts, J. M., Fehsenfeld, F. C., Worsnop, D. R., Canagaratna, M. R., Pszenny, A. A. P., Keene, W. C., Marchewka, M., Bertman, S. B., and Bates, T. S.: Budget of organic carbon in a polluted atmosphere: Results from the New England Air Quality Study in 2002, J. Geophys. Res.-Atmos., 110, D16305, doi:10.1029/2004jd005623, 2005.

de Gouw, J. A., Welsh-Bon, D., Warneke, C., Kuster, W. C., Alexander, L., Baker, A. K., Beyersdorf, A. J., Blake, D. R., Canagaratna, M., Celada, A. T., Huey, L. G., Junkermann, W., Onasch, T. B., Salcido, A., Sjostedt, S. J., Sullivan, A. P., Tanner, D. J., Vargas, O., Weber, R. J., Worsnop, D. R., Yu, X. Y., and Zaveri, R.: Emission and chemistry of organic carbon in the gas and aerosol phase at a sub-urban site near Mexico City in March 2006 during the MILAGRO study, Atmos. Chem. Phys., 9, 3425–3442, doi:10.5194/acp-9-3425-2009, 2009.

Donahue, N. M., Robinson, A. L., Stanier, C. O., and Pandis, S. N.: Coupled partitioning, dilution, and chemical aging of semivolatile organics, Environ. Sci. Technol., 40(8), 2635–2643, doi:10.1021/es052297c, 2006.

Doran, C.: Corrigendum to "The T1-T2 study: evolution of aerosol properties downwind of Mexico City" published in Atmos. Chem. Phys., 7, 1585–1598, 2007, Atmos. Chem. Phys.,

ACPD
10, 30205–30277, 2010

7, 2197–2198, 2007,
http://www.atmos-chem-phys.net/7/2197/2007/.
Dusanter, S., Vimal, D., Stevens, P. S., Volkamer, R., and Molina, L. T.: Measurements of OH and HO_2 concentrations during the MCMA-2006 field campaign – Part 1: Deployment of the Indiana University laser-induced fluorescence instrument, Atmos. Chem. Phys., 9, 1665–1685, doi:10.5194/acp-9-1665-2009, 2009.
Dzepina, K., Volkamer, R. M., Madronich, S., Tulet, P., Ulbrich, I. M., Zhang, Q., Cappa, C. D., Ziemann, P. J., and Jimenez, J. L.: Evaluation of recently-proposed secondary organic aerosol models for a case study in Mexico City, Atmos. Chem. Phys., 9, 5681–5709, doi:10.5194/acp-9-5681-2009, 2009.
Dzepina, K., Cappa, C. D., Volkamer, R. M., Madronich, S., DeCarlo, P. F., Zaveri, R. A., and Jimenez, J. L.: Modeling the Multiday Evolution and Aging of Secondary Organic Aerosol During MILAGRO 2006, Environ. Sci. Technol., in review, 2010.
Emmons, L. K., Apel, E. C., Lamarque, J.-F., Hess, P. G., Avery, M., Blake, D., Brune, W., Campos, T., Crawford, J., DeCarlo, P. F., Hall, S., Heikes, B., Holloway, J., Jimenez, J. L., Knapp, D. J., Kok, G., Mena-Carrasco, M., Olson, J., O'Sullivan, D., Sachse, G., Walega, J., Weibring, P., Weinheimer, A., and Wiedinmyer, C.: Impact of Mexico City emissions on regional air quality from MOZART-4 simulations, Atmos. Chem. Phys., 10, 6195–6212, doi:10.5194/acp-10-6195-2010, 2010.
Fast, J. D., de Foy, B., Acevedo Rosas, F., Caetano, E., Carmichael, G., Emmons, L., McKenna, D., Mena, M., Skamarock, W., Tie, X., Coulter, R. L., Barnard, J. C., Wiedinmyer, C., and Madronich, S.: A meteorological overview of the MILAGRO field campaigns, Atmos. Chem. Phys., 7, 2233–2257, doi:10.5194/acp-7-2233-2007, 2007.
Fast, J., Aiken, A. C., Allan, J., Alexander, L., Campos, T., Canagaratna, M. R., Chapman, E., DeCarlo, P. F., de Foy, B., Gaffney, J., de Gouw, J., Doran, J. C., Emmons, L., Hodzic, A., Herndon, S. C., Huey, G., Jayne, J. T., Jimenez, J. L., Kleinman, L., Kuster, W., Marley, N., Russell, L., Ochoa, C., Onasch, T. B., Pekour, M., Song, C., Ulbrich, I. M., Warneke, C., Welsh-Bon, D., Wiedinmyer, C., Worsnop, D. R., Yu, X.-Y., and Zaveri, R.: Evaluating simulated primary anthropogenic and biomass burning organic aerosols during MILAGRO: implications for assessing treatments of secondary organic aerosols, Atmos. Chem. Phys., 9, 6191–6215, doi:10.5194/acp-9-6191-2009, 2009.
Fast, J. D., Gustafson Jr., W. I., Chapman, E. G., Easter, R. C., Rishel, J., Zaveri, R. A., Grell, G., and Barth, M.: The Aerosol Modeling Testbed: A community tool to objectively evaluate

ACPD
10, 30205–30277, 2010

aerosol process modules, B. Am. Meteorol. Soc., to be published, 2011.
Friedl, M. A., Sulla-Menashe, D., Tan, B., Schneider, A., Ramankutty, N., Sibley, A., and Huang, X. M.: MODIS Collection 5 global land cover: Algorithm refinements and characterization of new datasets, Rem. Sens. Environ., 114, 168–182, doi:10.1016/j.rse.2009.08.016, 2010.
Giglio, L., Descloitres, J., Justice, C. O., and Kaufman, Y. J.: An enhanced contextual fire detection algorithm for MODIS, Rem. Sens. Environ., 87, 273–282, doi:10.1016/s0034-4257(03)00184-6, 2003.
Goldstein, A. H. and Galbally, I. E.: Known and unexplored organic constituents in the earth's atmosphere, Environ. Sci. Technol., 41, 1514–1521, 2007.
Grell, G. A., Peckham, S. E., Schmitz, R., McKeen, S. A., Frost, G., Skamarock, W. C., and Eder, B.: Fully coupled "online" chemistry within the WRF model, Atmos. Environ., 39, 6957–6975, doi:10.1016/j.atmosenv.2005.04.027, 2005.
Grieshop, A. P., Logue, J. M., Donahue, N. M., and Robinson, A. L.: Laboratory investigation of photochemical oxidation of organic aerosol from wood fires 1: measurement and simulation of organic aerosol evolution, Atmos. Chem. Phys., 9, 1263–1277, doi:10.5194/acp-9-1263-2009, 2009.
Guenther, A., Karl, T., Harley, P., Wiedinmyer, C., Palmer, P. I., and Geron, C.: Estimates of global terrestrial isoprene emissions using MEGAN (Model of Emissions of Gases and Aerosols from Nature), Atmos. Chem. Phys., 6, 3181–3210, doi:10.5194/acp-6-3181-2006, 2006.
Hallquist, M., Wenger, J. C., Baltensperger, U., Rudich, Y., Simpson, D., Claeys, M., Dommen, J., Donahue, N. M., George, C., Goldstein, A. H., Hamilton, J. F., Herrmann, H., Hoffmann, T., Iinuma, Y., Jang, M., Jenkin, M. E., Jimenez, J. L., Kiendler-Scharr, A., Maenhaut, W., McFiggans, G., Mentel, Th. F., Monod, A., Prévôt, A. S. H., Seinfeld, J. H., Surratt, J. D., Szmigielski, R., and Wildt, J.: The formation, properties and impact of secondary organic aerosol: current and emerging issues, Atmos. Chem. Phys., 9, 5155–5236, doi:10.5194/acp-9-5155-2009, 2009.
Heald, C. L., Jacob, D. J., Park, R. J., Russell, L. M., Huebert, B. J., Seinfeld, J. H., Liao, H., and Weber, R. J.: A large organic aerosol source in the free troposphere missing from current models, Geophys. Res. Lett., 32, L18809, doi:10.1029/2005gl023831, 2005.
Hildebrandt, L., Donahue, N. M., and Pandis, S. N.: High formation of secondary organic aerosol from the photo-oxidation of toluene, Atmos. Chem. Phys., 9, 2973–2986, doi:10.5194/acp-9-2973-2009, 2009.

ACPD
10, 30205–30277, 2010

Hodzic, A., Jimenez, J. L., Madronich, S., Aiken, A. C., Bessagnet, B., Curci, G., Fast, J., Lamarque, J.-F., Onasch, T. B., Roux, G., Schauer, J. J., Stone, E. A., and Ulbrich, I. M.: Modeling organic aerosols during MILAGRO: importance of biogenic secondary organic aerosols, Atmos. Chem. Phys., 9, 6949–6981, doi:10.5194/acp-9-6949-2009, 2009.

Hodzic, A., Jimenez, J. L., Madronich, S., Canagaratna, M. R., DeCarlo, P. F., Kleinman, L., and Fast, J.: Modeling organic aerosols in a megacity: potential contribution of semi-volatile and intermediate volatility primary organic compounds to secondary organic aerosol formation, Atmos. Chem. Phys., 10, 5491–5514, doi:10.5194/acp-10-5491-2010, 2010a.

Hodzic, A., Jimenez, J. L., Prévôt, A. S. H., Szidat, S., Fast, J. D., and Madronich, S.: Can 3-D models explain the observed fractions of fossil and non-fossil carbon in and near Mexico City?, Atmos. Chem. Phys., 10, 10997–11016, doi:10.5194/acp-10-10997-2010, 2010b.

Hoelzemann, J. J., Schultz, M. G., Brasseur, G. P., Granier, C., and Simon, M.: Global Wildland Fire Emission Model (GWEM): Evaluating the use of global area burnt satellite data, J. Geophys. Res.-Atmos., 109, D14s04, doi:10.1029/2003jd003666, 2004.

Jimenez, J. L., Canagaratna, M. R., Donahue, N. M., Prevot, A. S. H., Zhang, Q., Kroll, J. H., DeCarlo, P. F., Allan, J. D., Coe, H., Ng, N. L., Aiken, A. C., Docherty, K. S., Ulbrich, I. M., Grieshop, A. P., Robinson, A. L., Duplissy, J., Smith, J. D., Wilson, K. R., Lanz, V. A., Hueglin, C., Sun, Y. L., Tian, J., Laaksonen, A., Raatikainen, T., Rautiainen, J., Vaattovaara, P., Ehn, M., Kulmala, M., Tomlinson, J. M., Collins, D. R., Cubison, M. J., Dunlea, E. J., Huffman, J. A., Onasch, T. B., Alfarra, M. R., Williams, P. I., Bower, K., Kondo, Y., Schneider, J., Drewnick, F., Borrmann, S., Weimer, S., Demerjian, K., Salcedo, D., Cottrell, L., Griffin, R., Takami, A., Miyoshi, T., Hatakeyama, S., Shimono, A., Sun, J. Y., Zhang, Y. M., Dzepina, K., Kimmel, J. R., Sueper, D., Jayne, J. T., Herndon, S. C., Trimborn, A. M., Williams, L. R., Wood, E. C., Middlebrook, A. M., Kolb, C. E., Baltensperger, U., and Worsnop, D. R.: Evolution of Organic Aerosols in the Atmosphere, Science, 326, 1525–1529, doi:10.1126/science.1180353, 2009.

Kleinman, L. I., Springston, S. R., Daum, P. H., Lee, Y.-N., Nunnermacker, L. J., Senum, G. I., Wang, J., Weinstein-Lloyd, J., Alexander, M. L., Hubbe, J., Ortega, J., Canagaratna, M. R., and Jayne, J.: The time evolution of aerosol composition over the Mexico City plateau, Atmos. Chem. Phys., 8, 1559–1575, doi:10.5194/acp-8-1559-2008, 2008.

Kroll, J. H., Ng, N. L., Murphy, S. M., Flagan, R. C., and Seinfeld, J. H.: Secondary organic aerosol formation from isoprene photooxidation, Environ. Sci. Technol., 40, 1869–1877, doi:10.1021/es0524301, 2006.

ACPD
10, 30205–30277, 2010

Kroll, J. H., Smith, J. D., Che, D. L., Kessler, S. H., Worsnop, D. R., and Wilson, K. R.: Measurement of fragmentation and functionalization pathways in the heterogeneous oxidation of oxidized organic aerosol, Phys. Chem. Chem. Phys., 11, 8005–8014, doi:10.1039/b905289e, 2009.

Lane, T. E., Donahue, N. M., and Pandis, S. N.: Effect of NOx on secondary organic aerosol concentrations, Environ. Sci. Technol., 42, 6022–6027, doi:10.1021/es703225a, 2008.

Marley, N. A., Gaffney, J. S., Tackett, M., Sturchio, N. C., Heraty, L., Martinez, N., Hardy, K. D., Marchany-Rivera, A., Guilderson, T., MacMillan, A., and Steelman, K.: The impact of biogenic carbon sources on aerosol absorption in Mexico City, Atmos. Chem. Phys., 9, 1537–1549, doi:10.5194/acp-9-1537-2009, 2009.

MODIS Hotspot/Active Fire Detections, data set: MODIS Rapid Response Project, NASA/GSFC [producer], University of Maryland, Fire Information for Resource Management System [distributors], available on-line at http://maps.geog.umd.edu, 2002.

Mohr, C., Huffman, J. A., Cubison, M. J., Aiken, A. C., Docherty, K. S., Kimmel, J. R., Ulbricht, I. M., Hannigan, M., and Jimenez, J. L.: Characterization of Primary Organic Aerosol Emissions from Meat Cooking, Trash Burning, and Motor Vehicles with High-Resolution Aerosol Mass Spectrometry and Comparison with Ambient and Chamber Observations, Environ. Sci. Technol., 43, 2443–2449, doi:10.1021/es8011518, 2009.

Murphy, D. M., Cziczo, D. J., Froyd, K. D., Hudson, P. K., Matthew, B. M., Middlebrook, A. M., Peltier, R. E., Sullivan, A., Thomson, D. S., and Weber, R. J.: Single-particle mass spectrometry of tropospheric aerosol particles, J. Geophys. Res.-Atmos., 111, D23s32, doi:10.1029/2006jd007340, 2006.

Ng, N. L., Chhabra, P. S., Chan, A. W. H., Surratt, J. D., Kroll, J. H., Kwan, A. J., McCabe, D. C., Wennberg, P. O., Sorooshian, A., Murphy, S. M., Dalleska, N. F., Flagan, R. C., and Seinfeld, J. H.: Effect of NO_x level on secondary organic aerosol (SOA) formation from the photooxidation of terpenes, Atmos. Chem. Phys., 7, 5159–5174, doi:10.5194/acp-7-5159-2007, 2007a.

Ng, N. L., Kroll, J. H., Chan, A. W. H., Chhabra, P. S., Flagan, R. C., and Seinfeld, J. H.: Secondary organic aerosol formation from m-xylene, toluene, and benzene, Atmos. Chem. Phys., 7, 3909–3922, doi:10.5194/acp-7-3909-2007, 2007b.

Ng, N. L., Canagaratna, M. R., Zhang, Q., Jimenez, J. L., Tian, J., Ulbrich, I. M., Kroll, J. H., Docherty, K. S., Chhabra, P. S., Bahreini, R., Murphy, S. M., Seinfeld, J. H., Hildebrandt, L., Donahue, N. M., DeCarlo, P. F., Lanz, V. A., Prévôt, A. S. H., Dinar, E., Rudich, Y., and

ACPD
10, 30205–30277, 2010

Worsnop, D. R.: Organic aerosol components observed in Northern Hemispheric datasets from Aerosol Mass Spectrometry, Atmos. Chem. Phys., 10, 4625–4641, doi:10.5194/acp-10-4625-2010, 2010.

Pye, H. O. T. and Seinfeld, J. H.: A global perspective on aerosol from low-volatility organic compounds, Atmos. Chem. Phys., 10, 4377–4401, doi:10.5194/acp-10-4377-2010, 2010.

Robinson, A. L., Donahue, N. M., Shrivastava, M. K., Weitkamp, E. A., Sage, A. M., Grieshop, A. P., Lane, T. E., Pierce, J. R., and Pandis, S. N.: Rethinking organic aerosols: Semivolatile emissions and photochemical aging, Science, 315, 1259–1262, doi:10.1126/science.1133061, 2007.

Shrivastava, M. K., Lipsky, E. M., Stanier, C. O., and Robinson, A. L.: Modeling semivolatile organic aerosol mass emissions from combustion systems, Environ. Sci. Technol., 40, 2671–2677, doi:10.1021/es0522231, 2006.

Shrivastava, M. K., Lane, T. E., Donahue, N. M., Pandis, S. N., and Robinson, A. L.: Effects of gas particle partitioning and aging of primary emissions on urban and regional organic aerosol concentrations, J. Geophys. Res.-Atmos., 113, D18301, doi:10.1029/2007jd009735, 2008.

Slowik, J. G., Stroud, C., Bottenheim, J. W., Brickell, P. C., Chang, R. Y.-W., Liggio, J., Makar, P. A., Martin, R. V., Moran, M. D., Shantz, N. C., Sjostedt, S. J., van Donkelaar, A., Vlasenko, A., Wiebe, H. A., Xia, A. G., Zhang, J., Leaitch, W. R., and Abbatt, J. P. D.: Characterization of a large biogenic secondary organic aerosol event from eastern Canadian forests, Atmos. Chem. Phys., 10, 2825–2845, doi:10.5194/acp-10-2825-2010, 2010.

Song, J., Lei, W., Bei, N., Zavala, M., de Foy, B., Volkamer, R., Cardenas, B., Zheng, J., Zhang, R., and Molina, L. T.: Ozone response to emission changes: a modeling study during the MCMA-2006/MILAGRO Campaign, Atmos. Chem. Phys., 10, 3827–3846, doi:10.5194/acp-10-3827-2010, 2010.

Stone, E. A., Hedman, C. J., Zhou, J. B., Mieritz, M., and Schauer, J. J.: Insights into the nature of secondary organic aerosol in Mexico City during the MILAGRO experiment 2006, Atmos. Environ., 44, 312–319, doi:10.1016/j.atmosenv.2009.10.036, 2010.

Tsimpidi, A. P., Karydis, V. A., Zavala, M., Lei, W., Molina, L., Ulbrich, I. M., Jimenez, J. L., and Pandis, S. N.: Evaluation of the volatility basis-set approach for the simulation of organic aerosol formation in the Mexico City metropolitan area, Atmos. Chem. Phys., 10, 525–546, doi:10.5194/acp-10-525-2010, 2010.

Tunved, P., Hansson, H. C., Kerminen, V. M., Strom, J., Dal Maso, M., Lihavainen, H., Viisanen,

ACPD
10, 30205–30277, 2010

Y., Aalto, P. P., Komppula, M., and Kulmala, M.: High natural aerosol loading over boreal forests, Science, 312, 261–263, doi:10.1126/science.1123052, 2006.
Ulbrich, I. M., Canagaratna, M. R., Zhang, Q., Worsnop, D. R., and Jimenez, J. L.: Interpretation of organic components from Positive Matrix Factorization of aerosol mass spectrometric data, Atmos. Chem. Phys., 9, 2891–2918, doi:10.5194/acp-9-2891-2009, 2009.
Volkamer, R., Jimenez, J. L., San Martini, F., Dzepina, K., Zhang, Q., Salcedo, D., Molina, L. T., Worsnop, D. R., and Molina, M. J.: Secondary organic aerosol formation from anthropogenic air pollution: Rapid and higher than expected, Geophys. Res. Lett., 33, L17811, doi:10.1029/2006gl026899, 2006.
Wesely, M. L.: Parameterization of surface resistances to gaseous dry deposition in regional scale numerical models, Atmos. Environ., 23, 1293–1304, 1989.
Wiedinmyer, C., Quayle, B., Geron, C., Belote, A., McKenzie, D., Zhang, X. Y., O'Neill, S., and Wynne, K. K.: Estimating emissions from fires in North America for air quality modeling, Atmos. Environ., 40, 3419–3432, doi:10.1016/j.atmosenv.2006.02.010, 2006.
Zaveri, R. A., Easter, R. C., Fast, J. D., and Peters, L. K.: Model for Simulating Aerosol Interactions and Chemistry (MOSAIC), J. Geophys. Res.-Atmos., 113, D13204, doi:10.1029/2007jd008782, 2008.
Zhang, Q., Jimenez, J. L., Canagaratna, M. R., Allan, J. D., Coe, H., Ulbrich, I., Alfarra, M. R., Takami, A., Middlebrook, A. M., Sun, Y. L., Dzepina, K., Dunlea, E., Docherty, K., DeCarlo, P. F., Salcedo, D., Onasch, T., Jayne, J. T., Miyoshi, T., Shimono, A., Hatakeyama, S., Takegawa, N., Kondo, Y., Schneider, J., Drewnick, F., Borrmann, S., Weimer, S., Demerjian, K., Williams, P., Bower, K., Bahreini, R., Cottrell, L., Griffin, R. J., Rautiainen, J., Sun, J. Y., Zhang, Y. M., and Worsnop, D. R.: Ubiquity and dominance of oxygenated species in organic aerosols in anthropogenically-influenced Northern Hemisphere midlatitudes, Geophys. Res. Lett., 34, L13801, doi:10.1029/2007gl029979, 2007.

ACPD
10, 30205–30277, 2010

Table 1. Terminology used for various classes of organic species in this study.

	Gas phase organic compounds
SVOC	Semi-Volatile Organic Compounds: Primary organic vapors which have sufficiently low vapor pressure to dynamically partition between the gas and the aerosol phases (Robinson et al., 2007) i.e. $10^{-2} \leq C^* \leq 10^3\ \mu g\,m^{-3}$ at 298 K and 1 atm
IVOC	Intermediate Volatility Organic Compounds: Primary organic vapors with volatility higher than SVOC but lower the traditional VOCs i.e. $10^4 \leq C^* \leq 10^6\ \mu g\,m^{-3}$ at 298 K and 1 atm (Robinson et al., 2007)
S/IVOC	SVOC+IVOC
VOC	Volatile Organic Compounds: Gas-phase organic species with volatility higher than S/IVOC i.e. $C^* \geq 10^7\ \mu g\,m^{-3}$ at 298 K and 1 atm (e.g. toluene, isoprene, terpenes).
	Condensed phase organics
OA/TOTOA	Organic Aerosol: includes both primary and secondary mass components (POA+SOA defined below).
POA	Primary Organic Aerosol: defined as organic aerosol either directly emitted or formed due to condensation of organic vapors before photochemical oxidation in the atmosphere.
SOA	Secondary Organic Aerosol: defined as organic aerosol formed after photochemical oxidation and condensation of organic vapors (V – SOA + SI – SOA) in the atmosphere
V-SOA	Component of SOA formed due to photochemical oxidation of all VOC precursors (A – V – SOA + B – V – SOA described below)
A-V-SOA	Component of SOA formed due to photochemical oxidation of traditional anthropogenic VOC precursors (e.g. ARO1, ARO2, ALK4 etc.)
B-V-SOA	Component of SOA formed due to photochemical oxidation of biogenic VOC precursors (e.g. isoprene,monoterpenes,sesquiterpenes)
SI-SOA	Component of SOA formed due to photochemical oxidation of all S/IVOC precursors (A – SI – SOA + BB – SI – SOA)
A-SI-SOA	Component of SOA formed due to photochemical oxidation of anthropogenic S/IVOC precursors (e.g. traffic emissions, municipal trash burning)
BB-SI-SOA	Component of SOA formed due to photochemical oxidation of biomass burning S/IVOC precursors
	Aerosol Mass Spectrometer terminology
HOA ↔ POA	Hydrocarbon-like Organic Aerosols: an OA component identified with PMF which is consistent with mass spectral signatures of reduced species such as those from motor vehicle emissions. It is generally understood as a surrogate for urban combustion-related POA (Ulbrich et al., 2009).
OOA ↔ SOA	Oxygenated Organic Aerosols: an OA component identified with PMF which is characterized by its high oxygen content. It is generally understood as a surrogate for SOA from all sources.
BBOA	Biomass Burning Organic Aerosols: an OA component identified with PMF which is characterized by spectral features typical of biomass smoke. It is thought to be dominated by biomass burning POA, while biomass burning SOA is mostly apportioned into the OOA component.

ACPD
10, 30205–30277, 2010

Table 2. Factors (f_i) used to calculate S/IVOC emissions from POA.

C^* μg m^{-3} at 298 K	Biomass carbon (f_i)	Anthropogenic carbon (f_i)	ΔH_{vap} kJ mol^{-1}
0.01	0.09	0.23	112
0.1	0.18	0.17	106
1	0.27	0.26	100
10	0.42	0.40	94
100	0.54	0.51	88
1000	0.90	0.86	82
10^4	1.20	1.17	76
10^5	1.50	1.50	70
10^6	2.40	2.40	64

ACPD
10, 30205–30277, 2010

Table 3. SOA mass yields using a 4-product VBS with C^* of 1, 10, 100 and 1000 µg m^{-3} for V-SOA precursors.

V-SOA precursors	Aerosol yield high NO_x parameterization				Aerosol yield low NO_x parameterization			
	1	10	100	1000	1	10	100	1000
ALK4	N/A	0.038	N/A	N/A	N/A	0.075	N/A	N/A
ALK5	N/A	0.15	N/A	N/A	N/A	0.3	N/A	N/A
OLE1	0.001	0.005	0.038	0.15	0.005	0.009	0.06	0.225
OLE2	0.003	0.026	0.083	0.27	0.023	0.044	0.129	0.375
ARO1	0.01	0.24	0.45	0.7	0.01	0.24	0.7	0.7
ARO2	0.01	0.24	0.45	0.7	0.01	0.24	0.7	0.7
ISOP	0.001	0.023	0.015	0	0.009	0.03	0.015	0
TERP	0.012	0.122	0.201	0.5	0.107	0.092	0.359	0.6
SESQ	0.075	0.15	0.75	0.9	0.075	0.15	0.75	0.9

ACPD
10, 30205–30277, 2010

Table 4. Factors (f_i) used to calculate S/IVOC emissions from POA for 2-species VBS.

C^* µg m^{-3} at 298 K	Biomass or anthropogenic carbon (f_i)
0.01	1.0
10^5	6.5

ACPD
10, 30205–30277, 2010

Table 5. V-SOA 1-product mass yields.

V-SOA precursors	Aerosol yield high NO_x (1 µg m^{-3})	Aerosol yield low NO_x (1 µg m^{-3})	Reference
ARO1	0.08	0.304	Ng et al. (2007b)
ARO2	0.035	0.367	Ng et al. (2007b)
TERP	0.066	0.379	Ng et al. (2007a)
SESQ	0.847	0.417	Ng et al. (2007a)
ISOPRENE	0.038	0.01	Kroll et al. (2006)
ALK4	0.038	0.075	Tsimpidi et al. (2010)
ALK5	0.15	0.3	Tsimpidi et al. (2010)
OLE1	0.001	0.005	Tsimpidi et al. (2010)
OLE2	0.003	0.023	Tsimpidi et al. (2010)

ACPD
10, 30205–30277, 2010

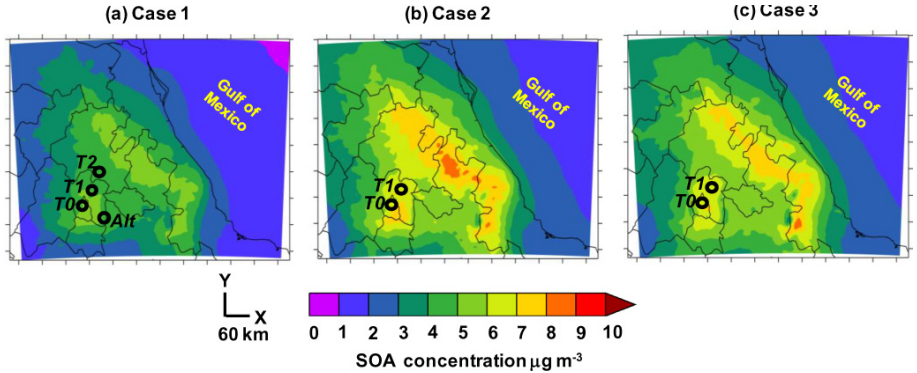

Fig. 1. Spatial distribution of 24-day average $PM_{2.5}$ SOA concentrations ($\mu g\,m^{-3}$) over Mexico City basin as predicted by 3 modeling Cases discussed in the text. Also indicated are locations of T0 site within city, T1 and T2 sites at the edge of the city, and the Altzomoni (Alt) site. Case 1 represents 9 species VBS with default emissions, while Case 2 and Case 3 represent 9 species and 2 species VBS respectively with twice anthropogenic S/IVOC emissions, as discussed in the text.

ACPD
10, 30205–30277, 2010

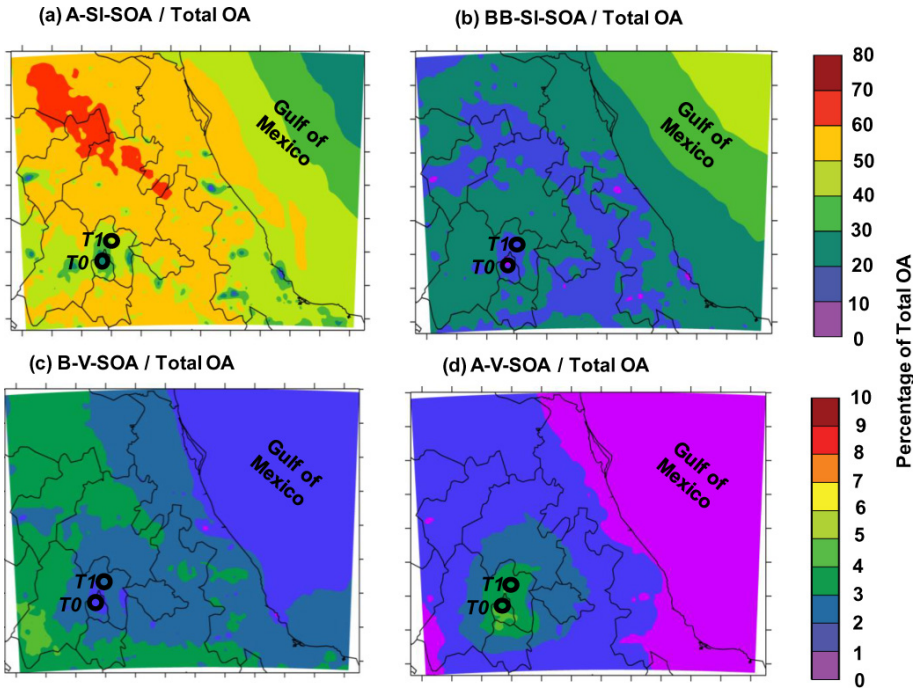

Fig. 2. Spatial distribution of 24-day average $PM_{2.5}$ SI-SOA components **(a)** anthropogenic A-SI-SOA; **(b)** biomass burning BB-SI-SOA; **(c)** biogenic B-V-SOA; **(d)** traditional anthropogenic A-V-SOA as a percentage of total OA over Mexico City basin as predicted by Case 2 (9-species VBS with twice default anthropogenic S/IVOC emissions).

ACPD
10, 30205–30277, 2010

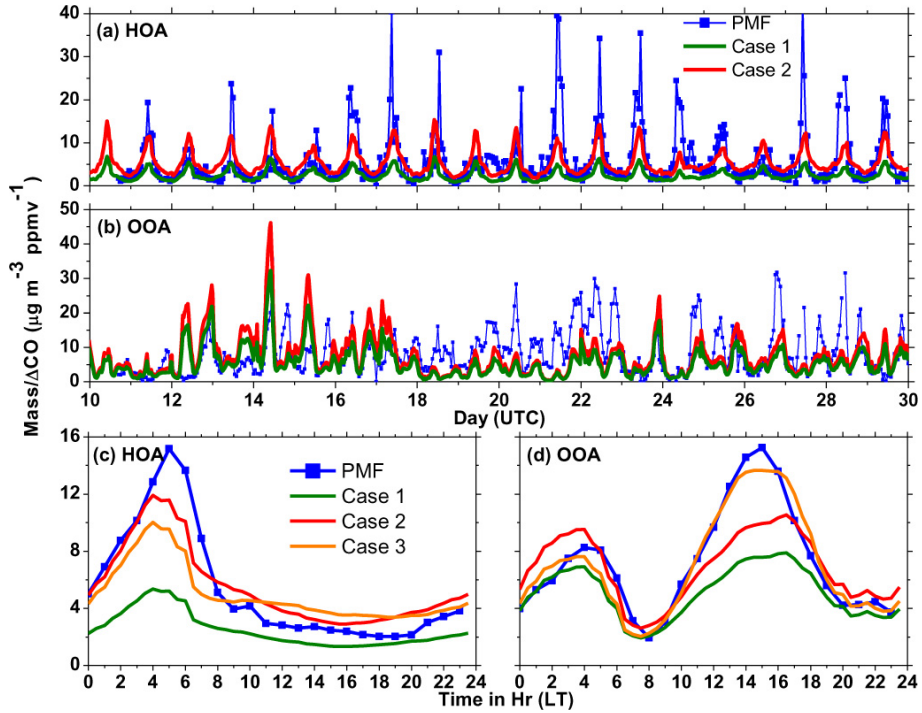

Fig. 3. Observed and simulated enhancement ratios of OA components with respect to CO at the T0 site within Mexico City for **(a)** HOA time series; **(b)** OOA time series; **(c)** HOA diurnal average; **(d)** OOA diurnal average. Case 3 is not shown in panels **(a)** and **(b)** as it is very similar to Case 2. ΔCO represents CO-50 ppb (assuming a background of 50 ppb) as discussed in text.

ACPD
10, 30205–30277, 2010

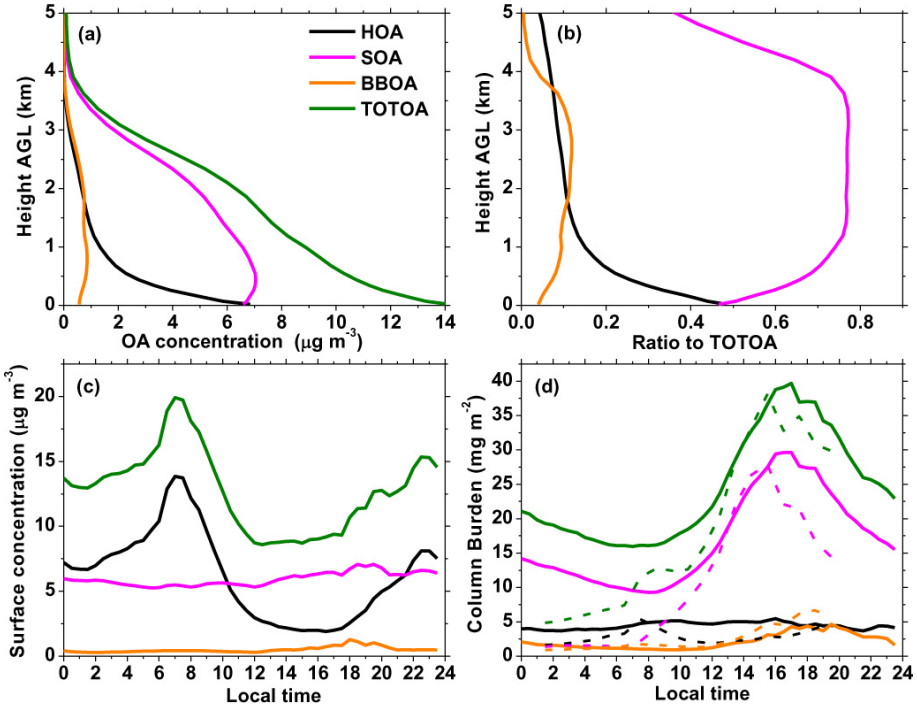

Fig. 4. 24 day averages over 6–30 March 2006 at T0 site predicted by Case 2 within Mexico City for **(a)** variation of OA concentration ($\mu g\,m^{-3}$) with height above ground level (a.g.l.); **(b)** ratio of HOA, SOA and BBOA from **(a)** with respect to TOTOA; **(c)** diurnal variation of surface concentrations (~25 m above ground level) of OA components; **(d)** diurnal variation of total column burden ($mg\,m^{-2}$) of OA components. Solid lines show Case 2 WRF-Chem simulations in the present study, while dashed lines show column burdens estimated by Aiken et al. (2010) over 10–31 March 2006 at T0 site for comparison.

ACPD
10, 30205–30277, 2010

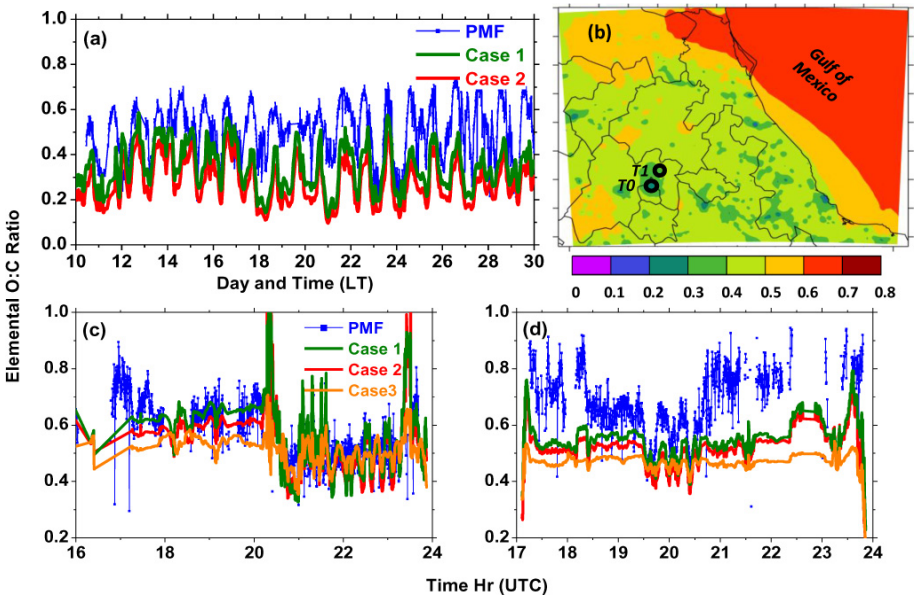

Fig. 5. Elemental O:C ratios over Mexico City region **(a)** time series of AMS and model (Case 1 and Case 2) results at T0 site for 10–30 March, **(b)** 24-day average spatial distribution at surface level for Case 2; **(c)** AMS and model results along C-130 flight track of 10 March morning; **(d)** same along C-130 flight track of 29 March morning.

ACPD
10, 30205–30277, 2010

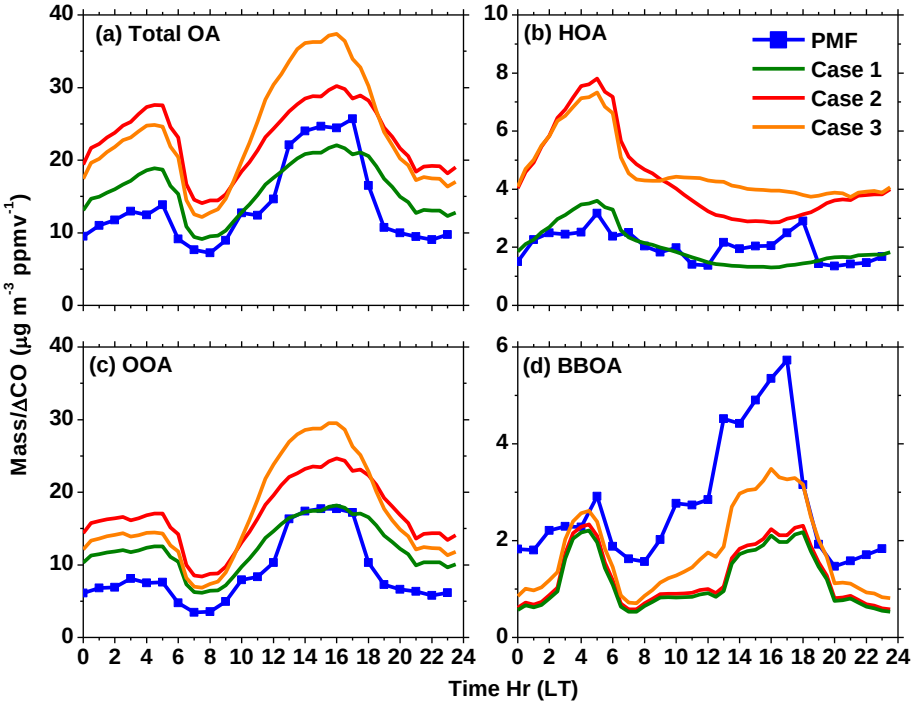

Fig. 6. Average diurnal observed and simulated enhancement ratios of OA components with respect to CO at the T1 site within Mexico City for **(a)** total OA; **(b)** HOA; **(c)** OOA; **(d)** BBOA. ΔCO represents CO-50 ppb (assuming a background of 50 ppb) as discussed in text.

ACPD
10, 30205–30277, 2010

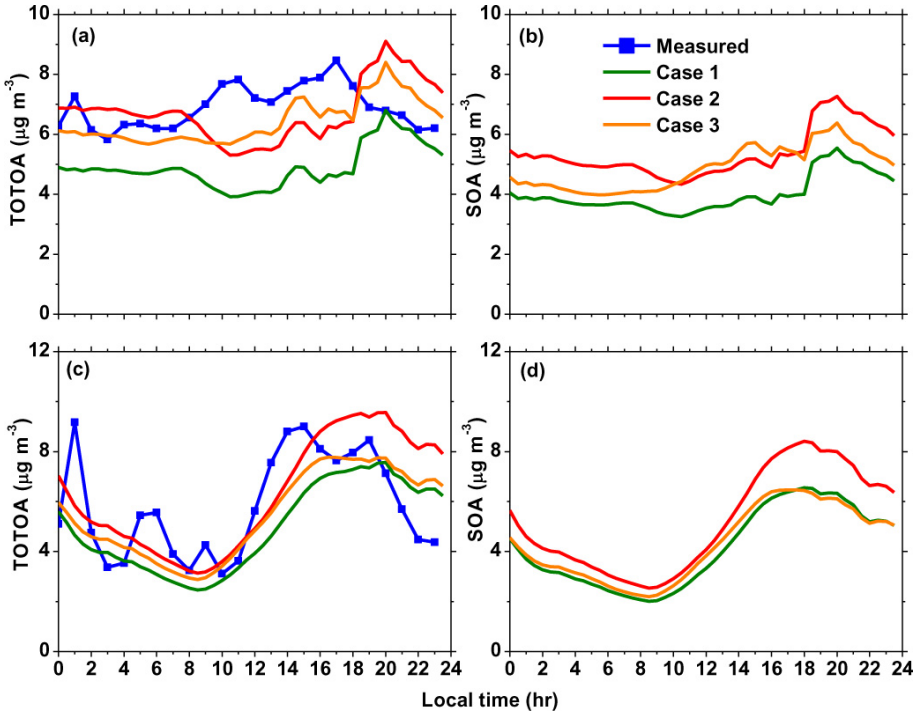

Fig. 7. Average diurnal observed and simulated concentrations of **(a)** TOTOA at T2 site; **(b)** SOA at T2 site; **(c)** TOTOA at Altzomoni mountain site; **(d)** SOA at Altzomoni mountain site. Location of T2 and Altzomoni sites are indicated in Fig. 1a.

ACPD
10, 30205–30277, 2010

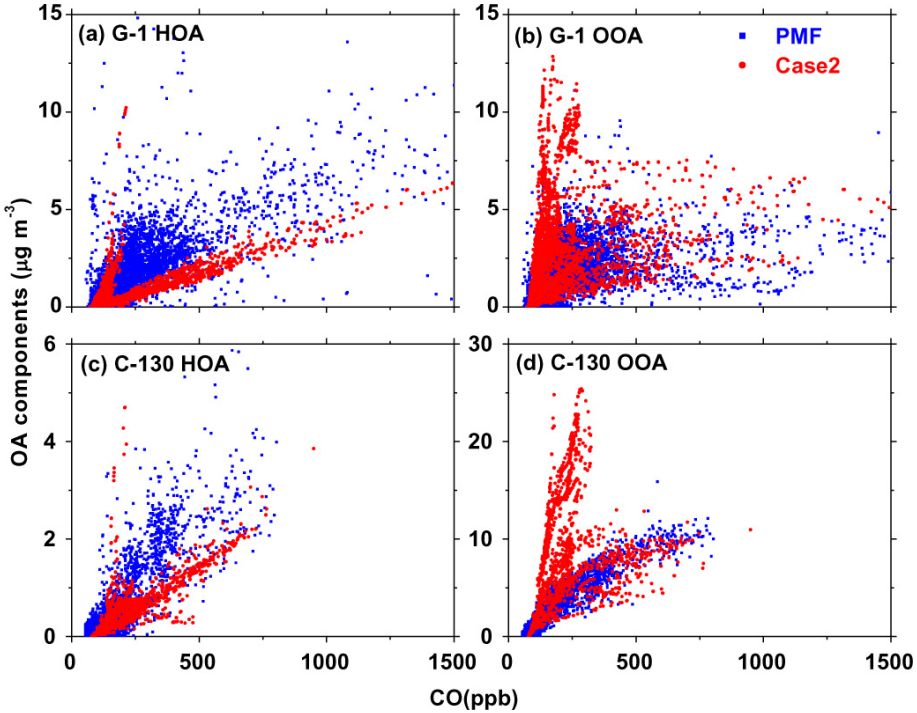

Fig. 8. WRF-Chem (Case 2) predictions of OA components vs. CO mixing ratios **(a)** HOA for 8 G1 flights; **(b)** OOA for 8 G-1 flights; **(c)** HOA for 2 C-130 flights; **(d)** OOA for 2 C130 flights.

ACPD
10, 30205–30277, 2010

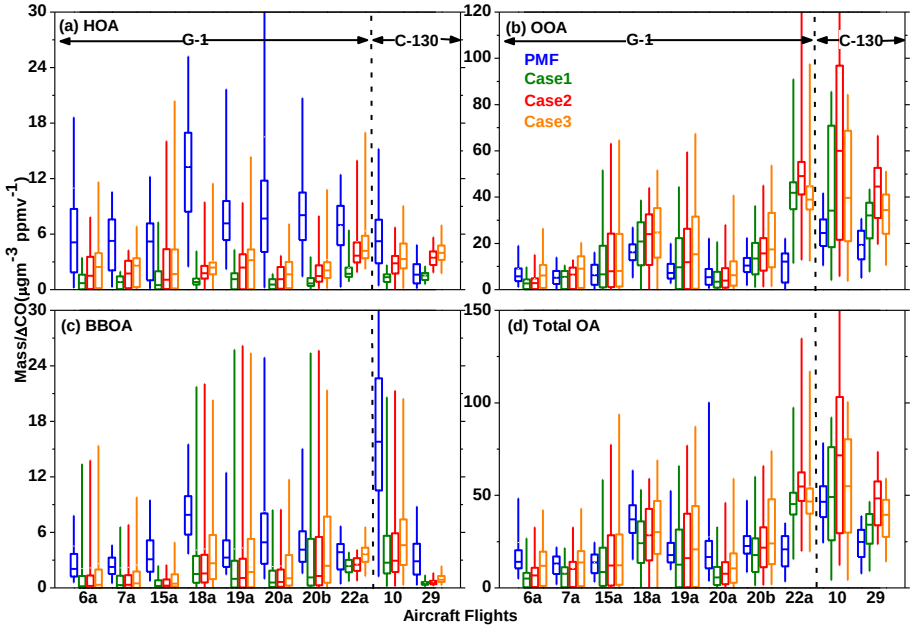

Fig. 9. Comparison of PMF components and WRF-Chem results (enhancement ratios with respect to CO) for the 3 modeling Cases along the 8 G-1 and 2 C-130 aircraft flight tracks where horizontal lines denote median, boxes denote 25th and 75th percentiles, and whiskers denote 5th and 95th percentiles for **(a)** HOA; **(b)** OOA; **(c)** BBOA; **(d)** total OA. ΔCO represents CO-50 ppb (assuming a background of 50 ppb) as discussed in text.

ACPD
10, 30205–30277, 2010

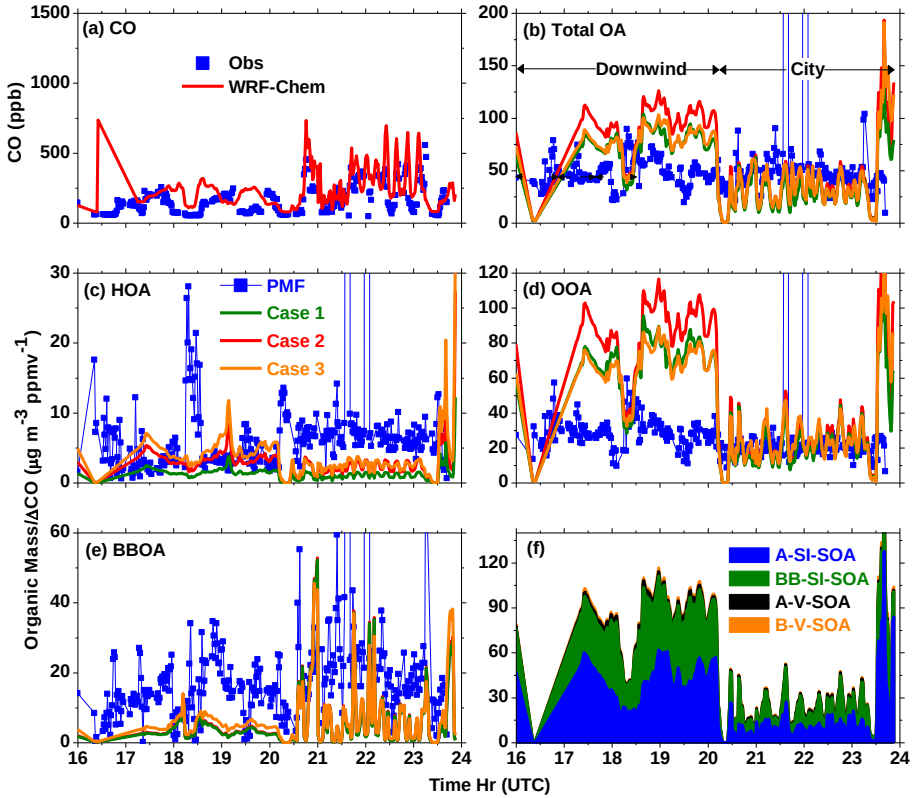

Fig. 10. Comparing simulated and measured **(a)** CO mixing ratios, and Enhancement ratios of **(b)** total OA, **(c)** HOA, **(d)** OOA and **(e)** BBOA versus corresponding PMF factors. **(f)** Various SOA components along flight transects of C-130 on 10 March as discussed in text.

ACPD
10, 30205–30277, 2010

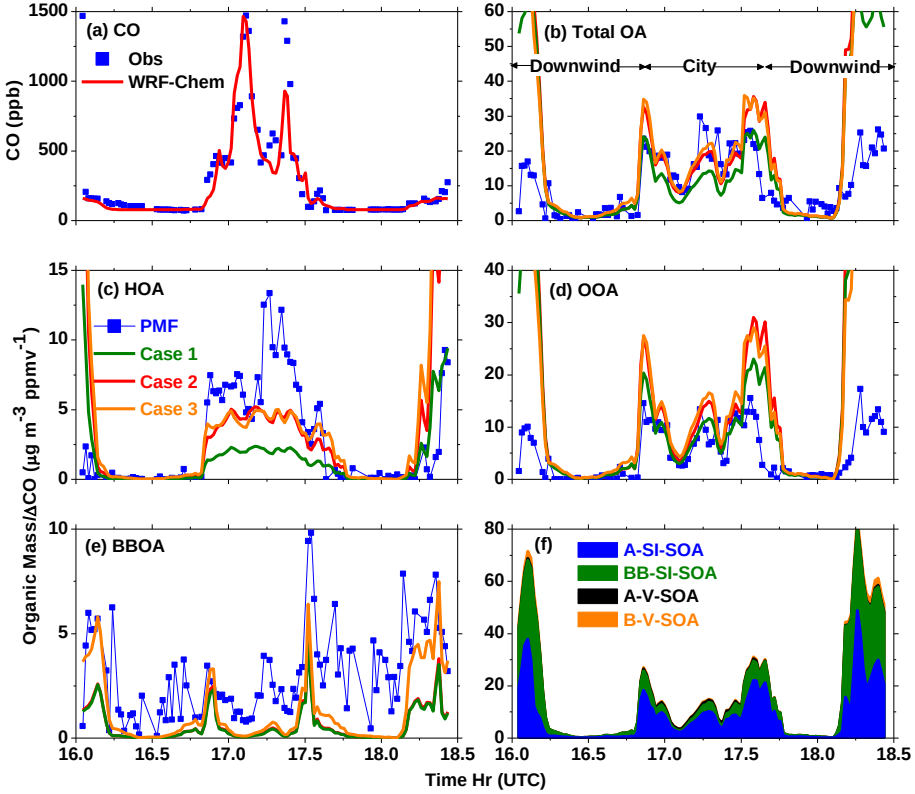

Fig. 11. Comparing simulated and measured **(a)** CO mixing ratios, and Enhancement ratios of **(b)** total OA, **(c)** HOA, **(d)** OOA and **(e)** BBOA versus corresponding PMF factors. **(f)** Various SOA components along flight transects of G-1 on 15 March as discussed in text.

ACPD
10, 30205–30277, 2010

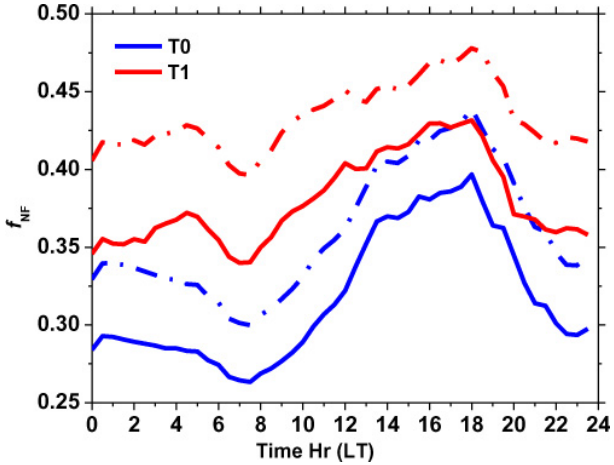

Fig. 12. Average diurnal variation of non-fossil carbon fraction (f_{NF}) at the T0 and T1 sites in Mexico City region for 6–30 March 2006. Solid lines represent Case 2 in this study, while dashed lines represent the same modeling Case (Case 2) with 5 times predicted biogenic B-V-SOA concentrations at T0 and T1 sites. Increasing biogenic SOA concentration by a factor of 5 increases predicted f_{NF} by 0.05 at both sites.

ACPD
10, 30205–30277, 2010

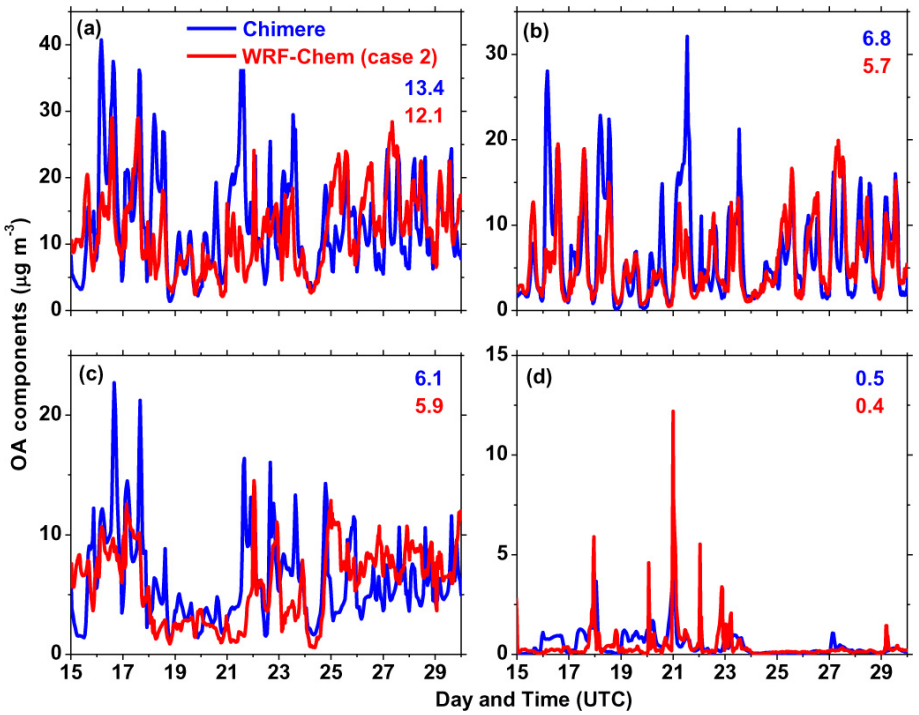

Fig. 13. Comparing predictions of **(a)** total OA, **(b)** HOA, **(c)** SOA and **(d)** BBOA from CHIMERE (using the ROB approach) vs. WRF-Chem model (Case 2) at the T0 site in Mexico City. The mean predicted values from the two models are also indicated.

ACPD
10, 30205–30277, 2010

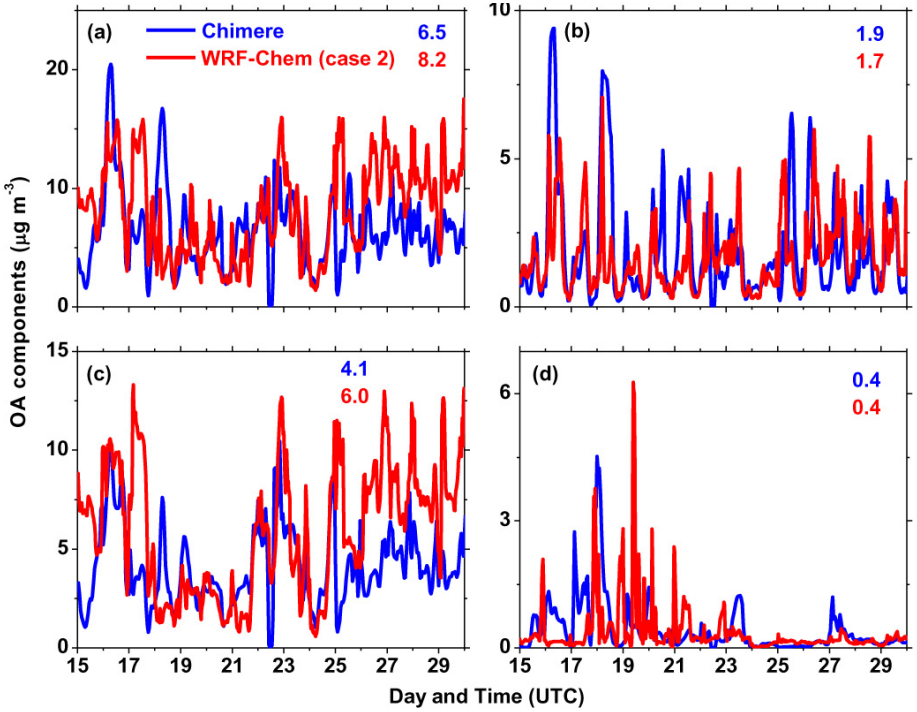

Fig. 14. Comparing predictions of **(a)** total OA, **(b)** HOA, **(c)** SOA and **(d)** BBOA from CHIMERE (using the ROB approach) vs. WRF-Chem model (Case 2) at the T1 site in Mexico City. The mean predicted values from the two models are also indicated.

ACPD
10, 30205–30277, 2010

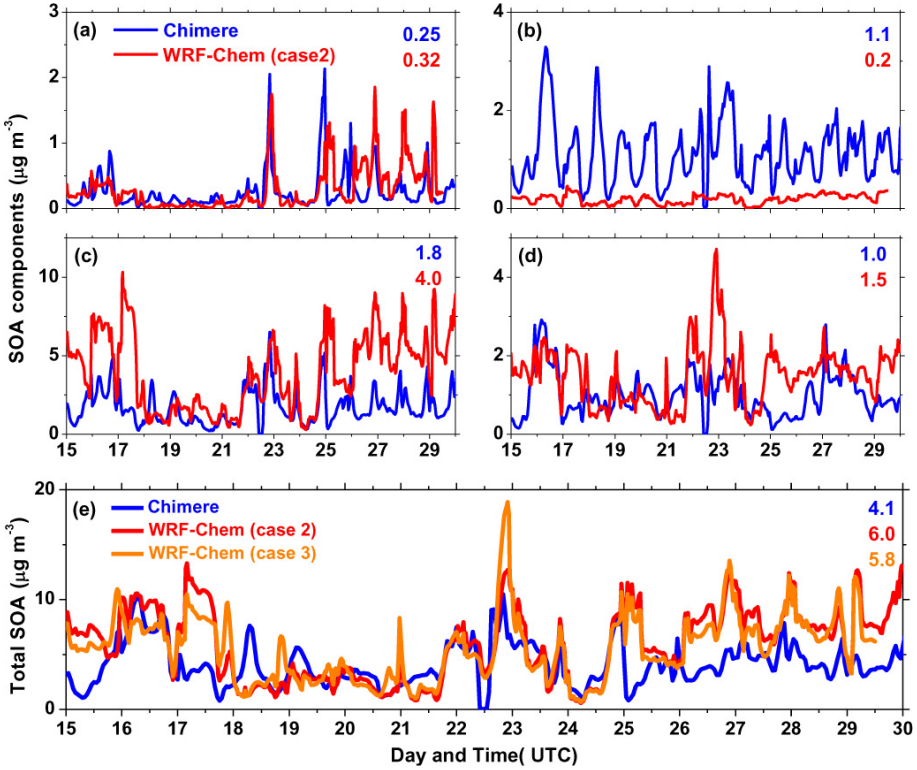

Fig. 15. Comparing predictions of SOA components from CHIMERE (using the ROB approach) vs. WRF-Chem model at the T1 site in Mexico City **(a)** traditional A-V-SOA; **(b)** biogenic B-V-SOA; **(c)** anthropogenic A-SI-SOA; **(d)** biomass burning BB-SI-SOA; **(e)** total SOA. Temporally averaged values are also indicated on each figure.

ACPD
10, 30205–30277, 2010